Combining bond particles with the Gutzwiller approximation: A variational theory of the Kondo lattice

M. Keßler and R. Eder
Karlsruher Institut für Technologie, Institute for Quantum Materials and Technologies, 76021 Karlsruhe, Germany

(Received 29 April 2022; revised 30 June 2022; accepted 8 July 2022; published 19 July 2022)

We investigate the two-dimensional Kondo lattice, the minimal model of a heavy fermion compound. Despite its apparent simplicity, its dynamics are both complex and controversial. In the moderate-to-strong coupling regime, the bond fermion theory provides an approximate mapping to an easily solvable fermionic system. This works surprisingly well from a qualitative standpoint, but there are some shortcomings as the method has no precise mathematical foundation. We here try to address this and improve on the method by making an explicit connection to wave function based variational methods and the Gutzwiller approximation. We apply the improved method to both the previously studied Néel magnetic phases, as well as incommensurately and ferromagnetically ordered phase.

DOI: 10.1103/PhysRevB.106.045122

I. THE KONDO LATTICE AND BOND FERMION THEORY

The notion of *heavy fermion* systems includes a large class of compounds. While their features are similarly varied, the common thread are the massive (in the Fermi liquid sense) excitation bands they derive their names from. Generally speaking, they have shown to be remarkably malleable, with phase transitions induced by tuning a number of distinct external parameters like pressure, doping, or magnetic field strength. An introduction can be found in Ref. [1], so we will only briefly recapitulate a few of the main features of these compounds, focusing on their magnetically ordered phases.

The typical arrangement in a heavy fermion system is the combination of local magnetic moments provided by partially filled ionic $4f$ or $5f$ shells, and one or more conducting electron bands. The important component responsible for the system's interesting properties is the non-negligible interaction between conduction electrons and local moments. As was pointed out by Doniach [2], coupling results in two competing mechanisms. One of them is *Kondo screening* [3], the appearance of bound states. Local moments "capture" conduction electrons to form localized states that have zero net magnetic moment. The other mechanism is the indirect *RKKY interaction* [4] between local moments, which is mediated by conduction electrons and drives the system toward magnetic order. Kondo screening impedes this, since only unscreened moments can take part in the Ruderman-Kittel-Kasuya-Yosida (RKKY) interaction. Whether the system is ordered or disordered thus depends on the interplay and relative strengths of both effects.

The simplest models that include these features are the *periodic Anderson model* (PAM) and its limiting case, the *Kondo lattice model* [5]. In its most basic form, the PAM consists of a single band of conduction (c) electrons on a lattice, each site also holding an (f) orbital that models localized (ionic) electron states. Physically, these localized states are strongly correlated, which is modeled by a Hubbard repulsion parameter U. Hybridization between c and f states leads to an effective magnetic interaction, characteristic of a heavy fermion system.

The Kondo lattice arises through a Schrieffer-Wolf transformation in the limit of large U [5]. The interaction fixes the occupation of the f orbitals: Excited states with zero or two f electrons are eliminated, resulting in localized spins interacting with the c electrons through a residual Heisenberg exchange.

While many extensions to these models are possible, we will investigate the basic Kondo lattice model on a two-dimensional square lattice.

Even this quite minimal model remains strongly nontrivial and has been the subject of many studies, which we roughly divide into mean-field type [6–18] and other (numerical) [19–38] approaches. Exact results are only available in special cases: For example, in the half-filled case, the numerically exact quantum Monte Carlo (QMC) results by Assaad [24] show that a phase transition takes place between a Néel phase at small interaction and a Kondo screened phase at large interaction.

Bond fermion theory is an approximate strong-coupling theory intended to describe the correlated states of the Kondo lattice [39]. The insulating Kondo screened phase, formed when the interaction is much larger than the hopping strength, is taken as a "background" state. Excitations generated by the hopping terms in the Hamiltonian are regarded as effective (bond) particles. While one can formulate this mapping exactly from an operator viewpoint [40,41], the resulting theory is an interacting system of bosons and fermions subject to a local constraint. Solving such a system is intractable without further approximation. Alternatively, one can focus solely on the fermionic degrees of freedom from the start. Previously, some steps in the procedure were only intuitively (instead of mathematically) justified. Nonetheless, this version of

the method has been applied to both paramagnetic [39], antiferromagnetic [42], and geometrically frustrated systems [43]. Especially in the first two cases, the results compare reasonably well to numerical calculations, taking into account the bond fermion method's simplicity.

Here we develop the bond fermion method further by re-examining its underlying mathematical formulation. At the cost of increasing the complexity of the method somewhat, its numerical accuracy is improved significantly. Some approximations are still uncontrolled, but they are now explicitly and mathematically formulated. We apply this method to the square lattice and its (planar) magnetic phases, both commensurate and incommensurate.

II. BOND FERMIONS AS A VARIATIONAL THEORY

The Kondo lattice Hamiltonian is

$$H = H_t + H_J, \tag{1}$$

$$H_t = -\sum_{\mathbf{R}\mathbf{R}'} t_{\mathbf{R}\mathbf{R}'} c^\dagger_{\mathbf{R}} c_{\mathbf{R}'}, \tag{2}$$

$$H_J = \sum_{\mathbf{R}} J \mathbf{S}^c_{\mathbf{R}} \mathbf{S}^f_{\mathbf{R}}, \tag{3}$$

$$\mathbf{S}^c_{\mathbf{R}} = c^\dagger_{\mathbf{R}} \frac{\boldsymbol{\sigma}}{2} c_{\mathbf{R}}, \tag{4}$$

$$c_{\mathbf{R}} = (c_{\mathbf{R}\uparrow} \quad c_{\mathbf{R}\downarrow})^\intercal. \tag{5}$$

$c^\dagger_{\mathbf{R}\sigma}$ creates a conduction electron of spin σ at site $\mathbf{R}$, while $\mathbf{S}^f_{\mathbf{R}}$ is the spin-1/2 operator of the local moment at $\mathbf{R}$. Instead of an explicit spin operator, we can equivalently introduce electron operators $f^\dagger_{\mathbf{R}\sigma}$ that in turn create the local moments. For this to yield the same dynamics as a bare spin, we have to introduce the constraint that each site is occupied by exactly one f electron. We do not include an explicit nonlocal interaction between f electrons $\propto \mathbf{S}^f_{\mathbf{R}} \mathbf{S}^f_{\mathbf{R}'}$ (the so-called Kondo-Heisenberg model) for reasons we will discuss later.

With a Fourier transform, the kinetic energy Hamiltonian yields the free band structure

$$H_t = \sum_{\mathbf{k}} \epsilon_{\mathbf{k}} c^\dagger_{\mathbf{k}} c_{\mathbf{k}}, \tag{6}$$

$$\epsilon_{\mathbf{k}} = -2t(\cos(k_x) + \cos(k_y)) + 4t' \cos(k_x)\cos(k_y). \tag{7}$$

t and t' respectively denote the first- and second-nearest neighbor hopping constants, with $t' = 0$ the particle-hole symmetric case. The $\mathbf{k}$ sum ranges over the usual square lattice Brillouin zone. Where not stated explicitly, we use t as our unit of energy.

The local Hilbert space of the Kondo lattice consists of eight states. Two of these have zero conduction electrons, and two others describe double occupations. Each of these two sets of states forms a spin-1/2 doublet (the spin being carried by the localized electron), which we will refer to as A_σ and B_σ respectively. The other four states describe states with a single c electron, and can be further divided into a spin-0 singlet (S) and a spin-1 triplet ($\mathbf{T}$). Explicitly, the basis states of site $\mathbf{R}$ are

$$|A_\sigma\rangle_{\mathbf{R}} = f^\dagger_{\mathbf{R}\sigma} |0\rangle_{\mathbf{R}}, \tag{8}$$

$$|B_\sigma\rangle_{\mathbf{R}} = f^\dagger_{\mathbf{R}\sigma} c^\dagger_{\mathbf{R}\uparrow} c^\dagger_{\mathbf{R}\downarrow} |0\rangle_{\mathbf{R}}, \tag{9}$$

$$|S\rangle_{\mathbf{R}} = \frac{1}{\sqrt{2}} c^\dagger_{\mathbf{R}}\, i\tau_y\, f^*_{\mathbf{R}} |0\rangle_{\mathbf{R}}, \tag{10}$$

$$|\mathbf{T}\rangle_{\mathbf{R}} = \frac{1}{\sqrt{2}} c^\dagger_{\mathbf{R}}\, \boldsymbol{\tau} i\tau_y\, f^*_{\mathbf{R}} |0\rangle_{\mathbf{R}}. \tag{11}$$

Here we used $|0\rangle_{\mathbf{R}}$ to denote the vacuum state of site $\mathbf{R}$, in which neither the localized nor the conduction electron states are occupied. $f^*_{\mathbf{R}}$ should be understood as $(f^\dagger_{\mathbf{R}})^\intercal$, i.e., the column vector of creation operators. The $\mathbf{T}$ transform as a spin-1 vector under spin rotations.

These basis vectors are eigenstates of the exchange term

$$J\mathbf{S}^c_{\mathbf{R}} \mathbf{S}^f_{\mathbf{R}} |S\rangle_{\mathbf{R}} = -\tfrac{3}{4} J |S\rangle_{\mathbf{R}}, \tag{12}$$

$$J\mathbf{S}^c_{\mathbf{R}} \mathbf{S}^f_{\mathbf{R}} |\mathbf{T}\rangle_{\mathbf{R}} = \tfrac{1}{4} J |\mathbf{T}\rangle_{\mathbf{R}}. \tag{13}$$

To construct our variational wave function, we form a linear combination of these four states. While the singlet state $|S\rangle_{\mathbf{R}}$ is favored at strong interaction, we will allow admixing of the triplet states to describe magnetic ordering. We write

$$|\Omega\rangle_{\mathbf{R}} = s_{\mathbf{R}} |S\rangle_{\mathbf{R}} + \mathbf{t}_{\mathbf{R}} |\mathbf{T}\rangle_{\mathbf{R}}, \tag{14}$$

$$1 = s^*_{\mathbf{R}} s_{\mathbf{R}} + \mathbf{t}^*_{\mathbf{R}} \mathbf{t}_{\mathbf{R}}. \tag{15}$$

The vector $\mathbf{t}_{\mathbf{R}}$ loosely corresponds to the ordered magnetic moment. We will take $s_{\mathbf{R}}$ and $\mathbf{t}_{\mathbf{R}}$ to be real and choose a spiral form

$$s_{\mathbf{R}} = s = \sqrt{1 - |\mathbf{t}|^2}, \tag{16}$$

$$\mathbf{t}_{\mathbf{R}} = |\mathbf{t}|(\cos(\mathbf{Q}\mathbf{R})\hat{e}_x + \sin(\mathbf{Q}\mathbf{R})\hat{e}_y). \tag{17}$$

$\mathbf{Q}$ is the magnetic wave vector. Néel antiferromagnetism has $\mathbf{Q} = (\pi, \pi)$, while pure ferromagnetic order has $\mathbf{Q} = (0, 0)$. s and $|\mathbf{t}|$ are constant, so that there is no modulation of the spin magnitude or of the charge density.

The ansatz (17) breaks both spin rotation and translation invariance, as would any finite and nonconstant $\mathbf{t}_{\mathbf{R}}$. However, there is a remaining symmetry: The system is unchanged when translating by $\mathbf{R}$ and simultaneously rotating the spins by $\varphi_{\mathbf{R}} = -\mathbf{Q}\mathbf{R}$ around the z axis. We therefore perform a canonical transformation that will result in a translation-invariant system. We introduce new electron operators c' and f' as

$$c^\dagger_{\mathbf{R}\sigma} = e^{-i\varphi_{\mathbf{R}}\frac{\sigma}{2}} c'^\dagger_{\mathbf{R}\sigma} = e^{i\mathbf{Q}\mathbf{R}\frac{\sigma}{2}} c'^\dagger_{\mathbf{R}\sigma}, \tag{18}$$

and equivalently for f. By replacing electron operators with their primed equivalents in (8)–(11) we get the new basis states

$$|S'\rangle_{\mathbf{R}} = |S\rangle_{\mathbf{R}}, \tag{19}$$

$$|T'_z\rangle_{\mathbf{R}} = |T_z\rangle_{\mathbf{R}}, \tag{20}$$

$$|T'_x\rangle_{\mathbf{R}} = \cos(\mathbf{Q}\mathbf{R})|T_x\rangle_{\mathbf{R}} + \sin(\mathbf{Q}\mathbf{R})|T_y\rangle_{\mathbf{R}}, \tag{21}$$

$$|T'_y\rangle_{\mathbf{R}} = \cos(\mathbf{Q}\mathbf{R})|T_y\rangle_{\mathbf{R}} - \sin(\mathbf{Q}\mathbf{R})|T_x\rangle_{\mathbf{R}}. \tag{22}$$

S and T_z are unchanged while T_x and T_y are rotated into each other, as to be expected from a spin-1 vector. A_σ and B_σ transform as spin-1/2 states (like $f^\dagger_{\mathbf{R}\sigma}$). Under this definition, (17) gives

$$\mathbf{t}_\mathbf{R}|\mathbf{T}\rangle_\mathbf{R} = |\mathbf{t}||T'_x\rangle_\mathbf{R}. \tag{23}$$

We now set

$$s'_\mathbf{R} = s' = s, \tag{24}$$

$$\mathbf{t}'_\mathbf{R} = |\mathbf{t}|\hat{e}_x, \tag{25}$$

which lets us recover $|\Omega\rangle_\mathbf{R}$ as

$$|\Omega\rangle_\mathbf{R} = s'_\mathbf{R}|S'\rangle_\mathbf{R} + \mathbf{t}'_\mathbf{R}|\mathbf{T}'\rangle_\mathbf{R}. \tag{26}$$

This has the exact same form as (14). However, in the primed frame the magnetic moment is constant and parallel to $\hat{e}_x$.

We also have to express the kinetic terms and the interaction using the primed operators. The interaction H_J is isotropic, so its form is unchanged. Regarding the kinetic energy, we see from (18) that

$$c^\dagger_{\mathbf{k}\sigma} = c'^\dagger_{\mathbf{k}+\frac{\mathbf{Q}\sigma}{2}}, \tag{27}$$

$$H_t = \sum_\mathbf{k} c'^\dagger_\mathbf{k} \tilde{\epsilon}_\mathbf{k} c'_\mathbf{k}, \tag{28}$$

$$\tilde{\epsilon}_\mathbf{k} = \begin{pmatrix} \epsilon_{\mathbf{k}+\frac{\mathbf{Q}}{2}} & 0 \\ 0 & \epsilon_{\mathbf{k}-\frac{\mathbf{Q}}{2}} \end{pmatrix}. \tag{29}$$

$\tilde{\epsilon}_\mathbf{k}$ is the effective kinetic energy matrix in spin space, in which all dependence on $\mathbf{Q}$ is isolated. This is the main utility of the transformation, as the system is now effectively translation invariant again. In the original frame, the position dependence of $\mathbf{t}_\mathbf{R}$ has to be carried through the whole calculation. This is possible but inconvenient. Especially once we get to the Gutzwiller renormalization matrices $\sqrt{Z}$ and Λ later in the calculation, working in a translation invariant environment is much less effort.

The rest of the calculation will take place in the rotated system, so we will drop the primes from now on. In addition to the "base" states $|\Omega\rangle_\mathbf{R}$, we will also include $|A_\sigma\rangle_\mathbf{R}$ and $|B_\sigma\rangle_\mathbf{R}$ which respectively have zero or two conduction electrons. The variational basis $|i\rangle$ consists of the product states

$$|i\rangle = \bigotimes_\mathbf{R} |i\rangle_\mathbf{R}, \tag{30}$$

$$|i\rangle_\mathbf{R} \in \{|\Omega\rangle_\mathbf{R},\ |A_\sigma\rangle_\mathbf{R},\ |B_\sigma\rangle_\mathbf{R}\}. \tag{31}$$

From (8), we see that the excited (A_σ and B_σ) states contain an odd number of fermions, and are thus fermionic (anticommuting) in nature, while Ω contains an even number of fermions. Inspired by this, we can simplify calculations of expectation values by introducing Hubbard-like [44] "bookkeeping" operators $a^\dagger_{\mathbf{R}\sigma}$ and $b^\dagger_{\mathbf{R}\sigma}$ defined through

$$a^\dagger_{\mathbf{R}\sigma} = |A_\sigma\rangle\langle\Omega|_\mathbf{R}, \tag{32}$$

$$b^\dagger_{\mathbf{R}\sigma} = |B_\sigma\rangle\langle\Omega|_\mathbf{R}. \tag{33}$$

The notation on the right-hand sides means that the operator acts on site $\mathbf{R}$ and leaves all other sites unaffected. These operators are taken to anticommute at different sites, so that they describe fermions. We collect them in two-component vectors

$$a_\mathbf{R} = (a_{\mathbf{R}\uparrow} \quad a_{\mathbf{R}\downarrow})^\mathsf{T}, \tag{34}$$

$$b_\mathbf{R} = (b_{\mathbf{R}\uparrow} \quad b_{\mathbf{R}\downarrow})^\mathsf{T}. \tag{35}$$

The utility of these fermion operators is that they allow for a transparent notation. We define the "vacuum" as

$$|\Omega\rangle = \bigotimes_\mathbf{R} |\Omega\rangle_\mathbf{R}. \tag{36}$$

All states of the form (30) can be generated by successively applying the creation operators $a^\dagger_{\mathbf{R}\sigma}$ and $b^\dagger_{\mathbf{R}\sigma}$ to this vacuum state. Note, however, that the product of any two creation operators at the same site vanishes ($a^\dagger_{\mathbf{R}\sigma} b^\dagger_{\mathbf{R}\sigma} = 0$, for example), so these fermions are actually subject to a hard-core condition of no double occupancy. For this reason, a and b operators may not be treated as ordinary fermions when acting on the same site. For example,

$$a^\dagger_{\mathbf{R}\sigma} b_{\mathbf{R}\sigma} = |A_\sigma\rangle\langle\Omega|_\mathbf{R}\,|\Omega\rangle\langle B_\sigma|_\mathbf{R} = |A_\sigma\rangle\langle B_\sigma|_\mathbf{R}, \tag{37}$$

$$b_{\mathbf{R}\sigma} a^\dagger_{\mathbf{R}\sigma} = |\Omega\rangle\langle B_\sigma|_\mathbf{R}\,|A_\sigma\rangle\langle\Omega|_\mathbf{R} = 0, \tag{38}$$

$$a^\dagger_{\mathbf{R}\sigma} b_{\mathbf{R}\sigma} \neq -b_{\mathbf{R}\sigma} a^\dagger_{\mathbf{R}\sigma}. \tag{39}$$

While it is tempting to identify the hard-core fermion system with that of ordinary fermions (ones that allow multiple occupation) subject to an infinitely strong Hubbard repulsion, this should be postponed until after one has expressed the variational energy through hard-core fermions with their appropriate commutation rules.

For a given variational state $|\Psi\rangle$ [a superposition of the basis states $|i\rangle$ in (30)], we can evaluate expectation values of an (electron number conserving) single-site operator $O_\mathbf{R}$ by separately computing the contributions of each state:

$$\begin{aligned}\langle O_\mathbf{R}\rangle &= \omega_\mathbf{R}\langle\Omega|O_\mathbf{R}|\Omega\rangle_\mathbf{R} \\ &\quad + \sum_{\sigma\sigma'}\langle a^\dagger_{\mathbf{R}\sigma} a_{\mathbf{R}\sigma'}\rangle\langle A_\sigma|O_\mathbf{R}|A_{\sigma'}\rangle_\mathbf{R} \\ &\quad + \sum_{\sigma\sigma'}\langle b^\dagger_{\mathbf{R}\sigma} b_{\mathbf{R}\sigma'}\rangle\langle B_\sigma|O_\mathbf{R}|B_{\sigma'}\rangle_\mathbf{R},\end{aligned} \tag{40}$$

$$\omega_\mathbf{R} = 1 - \langle a^\dagger_\mathbf{R} a_\mathbf{R}\rangle - \langle b^\dagger_\mathbf{R} b_\mathbf{R}\rangle. \tag{41}$$

Simple angle brackets $\langle\cdot\rangle$ denote expectation values with respect to $|\Psi\rangle$. $\omega_\mathbf{R}$ is the probability that site $\mathbf{R}$ is in the "vacuum" state. Some useful expectation values are

$$\begin{aligned}\langle c^\dagger_\mathbf{R} c_\mathbf{R}\rangle &= \omega_\mathbf{R} + 2\langle b^\dagger_\mathbf{R} b_\mathbf{R}\rangle \\ &= 1 - \langle a^\dagger_\mathbf{R} a_\mathbf{R}\rangle + \langle b^\dagger_\mathbf{R} b_\mathbf{R}\rangle,\end{aligned} \tag{42}$$

$$\left\langle \mathbf{S}^c_\mathbf{R} \mathbf{S}^f_\mathbf{R}\right\rangle = \omega_\mathbf{R}\left(-\frac{3}{4}|s_\mathbf{R}|^2 + \frac{1}{4}|\mathbf{t}_\mathbf{R}|^2\right), \tag{43}$$

$$\left\langle \mathbf{S}^c_\mathbf{R}\right\rangle = \omega_\mathbf{R}\left(\Re s^*_\mathbf{R}\mathbf{t}_\mathbf{R} + \frac{i}{2}\mathbf{t}^*_\mathbf{R}\times\mathbf{t}_\mathbf{R}\right), \tag{44}$$

$$\begin{aligned}\left\langle \mathbf{S}^f_\mathbf{R}\right\rangle &= \omega_\mathbf{R}\left(-\Re s^*_\mathbf{R}\mathbf{t}_\mathbf{R} + \frac{i}{2}\mathbf{t}^*_\mathbf{R}\times\mathbf{t}_\mathbf{R}\right) \\ &\quad + \left\langle a^\dagger_\mathbf{R}\frac{\boldsymbol{\tau}}{2}a_\mathbf{R}\right\rangle + \left\langle b^\dagger_\mathbf{R}\frac{\boldsymbol{\tau}}{2}b_\mathbf{R}\right\rangle.\end{aligned} \tag{45}$$

From (42) we can see that a and b have the expected effect on the electron number, respectively decreasing or increasing it by one. Equation (43) gives us the Heisenberg interaction, which is now a simple quadratic function of the fermion operators. Note that in our case the total spin $(\mathbf{S}^c_{\mathbf{R}} + \mathbf{S}^f_{\mathbf{R}})$ is nonzero only in the fermion-like states, as we have $\mathbf{t}_{\mathbf{R}}$ real.

From (45), one can extrapolate that a Kondo-Heisenberg term $\mathbf{S}^f_{\mathbf{R}}\mathbf{S}^f_{\mathbf{R}'}$ would result in three kinds of bond fermion expectation values: a "background" term $\sim s_{\mathbf{R}}\mathbf{t}_{\mathbf{R}}s_{\mathbf{R}'}\mathbf{t}_{\mathbf{R}'}$ involving zero bond fermion operators, quadratic terms corresponding to the "field" felt by a bond fermion because of the ground-state polarization of the surrounding sites, and a nonlocal quartic term describing spin correlation between bond fermions on neighboring sites. To include such a f-f interaction in the Hamiltonian, one would thus have to deal with bond fermion interactions, possibly through mean-field theory if the term is small. In the more interesting case where the f-f interaction is comparable to the Kondo f-c interaction, triplet fluctuations are strong and cannot be ignored as in our calculation (see Ref. [45] for a bond particle treatment of a pure-spin model).

To calculate the kinetic energy, we must also consider nonlocal electron bilinears, i.e., expectation values with $\mathbf{R} \neq \mathbf{R}'$. These effectively factorize, where each electron is separately transformed into a sum of bond fermions before taking the expectation value [41]:

$$\langle c^\dagger_{\mathbf{R}\sigma} c_{\mathbf{R}'\sigma'}\rangle = \sum_{\alpha\alpha'} W^*_{\mathbf{R}\sigma\alpha} W_{\mathbf{R}'\sigma'\alpha'} \langle v^\dagger_{\mathbf{R}\alpha} v_{\mathbf{R}'\alpha'}\rangle, \tag{46}$$

$$v_{\mathbf{R}} = (a^\dagger_{\mathbf{R}\uparrow} \quad a^\dagger_{\mathbf{R}\downarrow} \quad b_{\mathbf{R}\uparrow} \quad b_{\mathbf{R}\downarrow})^{\mathsf{T}}, \tag{47}$$

$$W_{\mathbf{R}} = \frac{1}{\sqrt{2}}([s^*_{\mathbf{R}} + \mathbf{t}^*_{\mathbf{R}}\boldsymbol{\tau}]\, i\tau_y \qquad [-s_{\mathbf{R}} + \mathbf{t}_{\mathbf{R}}\boldsymbol{\tau}]). \tag{48}$$

The combined vector $v_{\mathbf{R}}$ is indexed by Greek letters and contains both creation and annihilation operators. $W_{\mathbf{R}\sigma\alpha}$ is a 2×4 matrix, with the index α ranging over the four components of $v_{\mathbf{R}}$. The $W_{\mathbf{R}}$ are used to "translate" electron hopping expectation values into bond fermion hopping expectation values. Note that $\langle c^\dagger_{\mathbf{R}\sigma} c_{\mathbf{R}'\sigma'}\rangle$ contains not only terms corresponding to bond fermion propagation (of the form $\langle a^\dagger_{\mathbf{R}\sigma} a_{\mathbf{R}'\sigma'}\rangle$ and $\langle b^\dagger_{\mathbf{R}\sigma} b_{\mathbf{R}'\sigma'}\rangle$), but also bond fermion pair creation or annihilation ($\langle a^\dagger_{\mathbf{R}\sigma} b^\dagger_{\mathbf{R}'\sigma'}\rangle$ and $\langle a_{\mathbf{R}\sigma} b_{\mathbf{R}'\sigma'}\rangle$). For later, it will be useful to note that $W_{\mathbf{R}}$ is real, as $t_y = 0$ in our specific case. To arrive at the above expression, it is allowed to anticommute bond fermion operators, as they act on different sites.

III. GUTZWILLER VARIATIONAL METHOD

In the previous section, we have rewritten all expectation values required to evaluate the variational energy as terms quadratic in a and b operators. While this takes care of the Heisenberg interaction, we now have to deal with the hard-core condition we imposed. As mentioned earlier, we do this by replacing the hard-core fermions with normal fermions subject to an infinite repulsion, as this cannot change the observables of the system. One should think of this as an entirely different system that happens to give the same results, and where expectation values take the same form as calculated in the previous section (which fixes the true ordering of fermion operators). However, now anticommutations as in (39) are allowed: While an intermediate state may have two fermions and thus infinite energy, it is still part of the new Hilbert space, so the operator does not have to vanish. Naturally, we will use the same symbols for a, b, etc., in the new system.

There has been some variety as to how previous calculation took the hard-core interaction into account. A different formulation of the bond fermion method was used by Jurecka and Brenig [40]. An equivalent of the hard-core condition also appears in their calculation, which they solved on the mean-field level. Alternatively, the most straightforward way is to simply ignore the interaction [42,43]. One can expect this to give reasonable results as long as the bond fermion concentration is low, which is the case near half-filling and strong coupling. Finally, a variety of approaches was tried in Ref. [41].

Instead of these choices, we will use a Gutzwiller wave function, a classic method first developed for the Hubbard model [46]. We expect this to yield a quantitative improvement of the results (for example, a better estimate of the critical interaction strength J_c for the onset of magnetic order) when compared to disregarding the hard-core interaction, while retaining the qualitatively good aspects of that calculation. In the Gutzwiller approach, the ground state is approximated by an uncorrelated (Slater determinant) wave function $|\Psi_0\rangle$, which is multiplied by a *Gutzwiller operator* P:

$$|\Psi_{\mathrm{G}}\rangle = P|\Psi_0\rangle. \tag{49}$$

In our case, the uncorrelated state $|\Psi_0\rangle$ is a state containing a and b fermions, so it is already nontrivial in this sense. In general, this state does not fulfill the hard-core constraint, and the role of P is to eliminate the forbidden multiple occupancies of bond fermions. As the resulting state is still difficult to work with, we use the well-known *Gutzwiller approximation* to calculate expectation values.

Metzner and Vollhardt [47] first demonstrated that expectation values of the Gutzwiller wave function (when applied to the Hubbard model) can be calculated exactly in the limit of a very large number of spatial dimensions. When this expression is used for finite-dimensional lattices, it coincides with the Gutzwiller approximation. Generally speaking, the same approximations can be derived by a slave boson mean field scheme originally put forward by Kotliar and Ruckenstein [48]. The slave boson scheme is simpler in the sense that one often arrives at the correct result more quickly, but we here outline the infinite-dimensions version of the calculation as we feel it is closer in spirit to our own wave function based approach.

There is some care to be taken because of the presence of pairing terms $a^\dagger_{\mathbf{R}\sigma} b^\dagger_{\mathbf{R}'\sigma'}$ in the hopping term (46), as they will also appear in the effective Hamiltonian. How to include such anomalous terms is described by Fabrizio [49], there in the context of superconductivity. We use this as a reference, but our calculation is easier because of the very simple form of the interaction.

The Gutzwiller operator is composed of a product of local projection operators

$$P = \prod_{\mathbf{R}} P_{\mathbf{R}}, \tag{50}$$

where $P_{\mathbf{R}}$ is only nonvanishing when acting on states with 0 or 1 bond fermions. Further, $P_{\mathbf{R}}$ should conserve the electron number, i.e., it should not mix a- and b-like states. We will also take it to be self-adjoint. To evaluate the Gutzwiller expectation values in infinite dimensions, some further constraints need to be enforced [49]:

$$\langle\Psi_0|P_{\mathbf{R}}\, P_{\mathbf{R}}|\Psi_0\rangle = \langle\Psi_0|\Psi_0\rangle = 1, \tag{51}$$

$$\langle\Psi_0|P_{\mathbf{R}}\, P_{\mathbf{R}}\, \mathcal{C}_{\mathbf{R}}|\Psi_0\rangle = \langle\Psi_0|\mathcal{C}_{\mathbf{R}}|\Psi_0\rangle, \tag{52}$$

where $\mathcal{C}_{\mathbf{R}}$ can stand for any local fermion bilinear. Substituting

$$\mathcal{C}_{\mathbf{R}} \;\to\; a^\dagger_{\mathbf{R}\sigma} b^\dagger_{\mathbf{R}\sigma'}, \tag{53}$$

we find that the left-hand side of (52) will necessarily vanish. This is because $a^\dagger_{\mathbf{R}\sigma} b^\dagger_{\mathbf{R}\sigma'}$ creates two fermions on the same site, which is not allowed. However, the right-hand side is in general nonzero: While the kinetic energy contains only *nonlocal* pair creation terms, a $|\Psi_0\rangle$ that minimizes this energy may well also have nonvanishing expectation values for *local* pair creation. To preclude this, we will restrict $|\Psi_0\rangle$ to states with

$$\langle a^\dagger_{\mathbf{R}\sigma} b^\dagger_{\mathbf{R}\sigma'}\rangle_0 = \langle a_{\mathbf{R}\sigma} b_{\mathbf{R}\sigma'}\rangle_0 = 0. \tag{54}$$

We use the notation $\langle\cdot\rangle_0$ for expectation values with respect to $|\Psi_0\rangle$, and $\langle\cdot\rangle$ for ones with respect to $|\Psi_{\mathrm{G}}\rangle$. In practice, we will use a set of Lagrange multipliers $\Lambda^0_{\sigma\sigma'}$ to enforce (54), each corresponding to a particular choice of σ and σ'. A topic related to this are the sum rules for electron expectation values; a discussion can be found in Appendix A.

We can now calculate $P_{\mathbf{R}}$. While this usually involves minimizing the Gutzwiller variational energy, the hard-core interaction and the constraints (51) and (52) together drastically simplify this procedure compared to the more general problem in Ref. [49]. In fact, they already provide enough information to uniquely determine $P_{\mathbf{R}}$. The calculation is easiest in the eigenbasis of the local density matrix

$$\rho_{\mathbf{R}} = \begin{pmatrix} \rho_{\mathbf{R}a} & 0 \\ 0 & \rho_{\mathbf{R}b} \end{pmatrix}, \tag{55}$$

$$\rho_{\mathbf{R}a} = \begin{pmatrix} \langle a^\dagger_\uparrow a_\uparrow\rangle_0 & \langle a^\dagger_\uparrow a_\downarrow\rangle_0 \\ \langle a^\dagger_\downarrow a_\uparrow\rangle_0 & \langle a^\dagger_\downarrow a_\downarrow\rangle_0 \end{pmatrix}. \tag{56}$$

$\rho_{\mathbf{R}b}$ is defined similarly. We introduce a four-component fermion vector $\xi_{\mathbf{R}}$ as

$$\begin{pmatrix} a_{\mathbf{R}\uparrow} \\ a_{\mathbf{R}\downarrow} \\ b_{\mathbf{R}\uparrow} \\ b_{\mathbf{R}\downarrow} \end{pmatrix} = U_{\mathbf{R}}\xi_{\mathbf{R}}, \tag{57}$$

$$U_{\mathbf{R}} = \begin{pmatrix} 0 & U_{\mathbf{R}a} \\ 0 & U_{\mathbf{R}b} \end{pmatrix}, \tag{58}$$

$$\langle\xi^\dagger_{\mathbf{R}i}\xi_{\mathbf{R}j}\rangle_0 = \langle N_{\mathbf{R}i}\rangle_0\delta_{ij}. \tag{59}$$

The former two components of ξ correspond to a, the latter to b. $N_{\mathbf{R}i}$ is the number operator of component i. $U_{\mathbf{R}a}$ and $U_{\mathbf{R}b}$ are two-dimensional spin-rotation matrices that respectively rotate the spins of the a and b fermions to the z axis. In a general setting, these rotations do not have to be the same, as the spin directions can be different. In our specific case, they both point in the x axis.

In this diagonal basis, the conditions (52) imply a similarly diagonal form for $P_{\mathbf{R}}$, meaning that it can be written solely in terms of the number operators $N_{\mathbf{R}i}$:

$$P_{\mathbf{R}} = p_{\mathbf{R}0}\prod_i \overline{N}_{\mathbf{R}i} + \sum_i p_{\mathbf{R}i} N_{\mathbf{R}i}\prod_{j\neq i}\overline{N}_{\mathbf{R}j}, \tag{60}$$

$$\overline{N}_{\mathbf{R}i} = 1 - N_{\mathbf{R}i}. \tag{61}$$

The first term is a projector onto the empty state, while each term in the sum projects onto a state with exactly one ξ occupied. $p_{\mathbf{R}0}$ and the $p_{\mathbf{R}i}$ are parameters that we need to solve for. Using this ansatz, (52) is automatically fulfilled for $\mathcal{C}_{\mathbf{R}} \to \xi^\dagger_{\mathbf{R}i}\xi_{\mathbf{R}j}$ with $i \neq j$ as both sides vanish. For $i = j$ ($\mathcal{C}_{\mathbf{R}} \to N_{\mathbf{R}i}$), a short calculation results in

$$p^2_{\mathbf{R}0} = \left(1 - \sum_i \langle N_{\mathbf{R}i}\rangle\right)\left(\prod_i \langle\overline{N}_{\mathbf{R}i}\rangle\right)^{-1}, \tag{62}$$

$$p^2_{\mathbf{R}i} = \left(\prod_{j\neq i}\langle\overline{N}_{\mathbf{R}j}\rangle\right)^{-1}, \tag{63}$$

so that $P_{\mathbf{R}}$ is determined completely.

It does not matter whether we take the expectation values on the right-hand side with respect to the Slater determinant or the Gutzwiller wave function. To see this, note that we can move $\mathcal{C}_{\mathbf{R}}$ on the left-hand side of (52) in between the two Gutzwiller operators, as $\mathcal{C}_{\mathbf{R}}$ and $P_{\mathbf{R}}$ commute for all operators with nonvanishing expectation values. Thus, we generally have

$$\langle\mathcal{C}_{\mathbf{R}}\rangle_0 = \langle\mathcal{C}_{\mathbf{R}}\rangle. \tag{64}$$

This will be used to evaluate the interaction energy.

Using the explicit form of $P_{\mathbf{R}}$, we can evaluate hopping expectation values using some of the formulas of Ref. [49]. For $\mathbf{R} \neq \mathbf{R}'$ the results are

$$\langle\xi^\dagger_i\xi_j\rangle = \sqrt{\zeta}_{\mathbf{R}i}\sqrt{\zeta}_{\mathbf{R}j}\langle\xi^\dagger_i\xi_j\rangle_0, \tag{65}$$

$$\langle\xi^\dagger_i\xi^\dagger_j\rangle = \sqrt{\zeta}_{\mathbf{R}i}\sqrt{\zeta}_{\mathbf{R}j}\langle\xi^\dagger_i\xi^\dagger_j\rangle_0. \tag{66}$$

Thereby, the renormalization constants are

$$\sqrt{\zeta}_{\mathbf{R}i} = \sqrt{\frac{1 - \sum_j\langle N_{\mathbf{R}j}\rangle}{1 - \langle N_{\mathbf{R}i}\rangle}}. \tag{67}$$

It is instructive to check some limiting values. For example, the hopping renormalizes to zero when the bond fermion density (the sum in the numerator) becomes unity. On the other hand, if only a single one of the $\langle N_{\mathbf{R}i}\rangle$ is finite, then numerator and denominator cancel and the hopping is not renormalized at all. This is also expected because alike fermions do not interact. Note that the expression in (67) is the same as the renormalization in Kotliar and Ruckenstein's slave boson theory when applied to a system with four fermion degrees of freedom [48].

It is now time to reverse the unitary transformation. We define the spin- and species-dependent renormalization matrix $\sqrt{Z}_{\mathbf{R}}$ as

$$\sqrt{Z}_{\mathbf{R}} = U_{\mathbf{R}}\sqrt{\zeta}_{\mathbf{R}}U_{\mathbf{R}}^{\dagger} = \begin{pmatrix} \sqrt{Z}_{\mathbf{R}a} & 0 \\ 0 & \sqrt{Z}_{\mathbf{R}b} \end{pmatrix}, \tag{68}$$

where $\sqrt{\zeta}_{\mathbf{R}}$ is the matrix with the $\sqrt{\zeta}_{\mathbf{R}i}$ on the diagonal. $\sqrt{Z}_{\mathbf{R}a}$ and $\sqrt{Z}_{\mathbf{R}b}$ are again two-dimensional matrices, as a and b fermions are not mixed as long as the electron number is conserved. This allows us to calculate intersite expectation values of the bond fermions as

$$\langle a_{\mathbf{R}\sigma}^{\dagger} a_{\mathbf{R}'\sigma'}\rangle = \sum_{\sigma_1\sigma_2} [\sqrt{Z}_{\mathbf{R}a}^{\dagger}]_{\sigma_1\sigma} [\sqrt{Z}_{\mathbf{R}'a}]_{\sigma'\sigma_2} \langle a_{\mathbf{R}\sigma_1}^{\dagger} a_{\mathbf{R}'\sigma_2}\rangle_0, \tag{69}$$

$$\langle a_{\mathbf{R}\sigma}^{\dagger} b_{\mathbf{R}'\sigma'}^{\dagger}\rangle = \sum_{\sigma_1\sigma_2} [\sqrt{Z}_{\mathbf{R}a}^{\dagger}]_{\sigma_1\sigma} [\sqrt{Z}_{\mathbf{R}b}^{\dagger}]_{\sigma_2\sigma'} \langle a_{\mathbf{R}\sigma_1}^{\dagger} b_{\mathbf{R}'\sigma_2}^{\dagger}\rangle_0, \tag{70}$$

etc.

Finally, we can write down the energy of the Gutzwiller state. Since $\mathbf{t}_{\mathbf{R}} = |\mathbf{t}|\hat{e}_x$ (in the canonically rotated system), both the translation matrix $W_{\mathbf{R}}$ and the renormalization matrix $\sqrt{Z}_{\mathbf{R}}$ are real symmetric and position independent. Combining (42) and (43) with (69) and (70), this results in the expectation value

$$\langle H\rangle = \langle H_J\rangle + \langle H_t\rangle, \tag{71}$$

$$\langle H_J\rangle = \sum_{\mathbf{R}} e[\langle a_{\mathbf{R}}^{\dagger} a_{\mathbf{R}}\rangle_0 + \langle b_{\mathbf{R}}^{\dagger} b_{\mathbf{R}}\rangle_0 - 1], \tag{72}$$

$$e = \frac{3J}{4}s^2 - \frac{J}{4}|\mathbf{t}|^2, \tag{73}$$

$$\langle H_t\rangle = \sum_{\mathbf{k}} \langle v_{\mathbf{k}}^{\dagger}\sqrt{Z}W^{\intercal}\tilde{\epsilon}_{\mathbf{k}}W\sqrt{Z}v_{\mathbf{k}}\rangle_0. \tag{74}$$

e is the energy needed to create a bond fermion. All terms in this expression depend only on the uncorrelated wave function, i.e., given a specific $|\Psi_0\rangle$ we can calculate $\sqrt{Z}$ and with it the energy.

To optimize the variational wave function, we take a similar route to Yao *et al.* [50]. The kinetic energy expectation value (74) depends nonlinearly on the expectation values of the bond fermions, as $\sqrt{Z}$ is itself a function of (local) expectation values. Optimization problems of this kind can be reframed as nonlinear eigenvalue problems by taking derivatives of the energy expectation value, which in turn yields an effective Hamiltonian that is subject to some self-consistency equation. The derivatives are collected in a matrix m. We also need to include the chemical potential μ to adjust the electron number to its correct value and a matrix of Lagrange multipliers Λ to enforce the constraints (54). Putting everything together, the effective Hamiltonian is

$$H_{\text{eff}} = \sum_{\mathbf{k}} v_{\mathbf{k}}^{\dagger}[h + \sqrt{Z}W^{\intercal}\tilde{\epsilon}_{\mathbf{k}}W\sqrt{Z}]v_{\mathbf{k}}, \tag{75}$$

$$h = e\,\mathrm{diag}(-1,-1,1,1) - \mu\,\mathrm{diag}(1,1,1,1) - \Lambda - m, \tag{76}$$

$$\Lambda = \begin{pmatrix} 0 & \Lambda_0 \\ \Lambda_0^{\intercal} & 0 \end{pmatrix}, \tag{77}$$

$$m = \begin{pmatrix} -m_a & 0 \\ 0 & m_b \end{pmatrix}, \tag{78}$$

$$[m_a]_{\sigma\sigma'} = \frac{2}{N}\sum_{\mathbf{k}} \left\langle v_{\mathbf{k}}^{\dagger} \frac{\partial\sqrt{Z}}{\partial\langle a_{\sigma}^{\dagger} a_{\sigma'}\rangle} W^{\intercal}\tilde{\epsilon}_{\mathbf{k}}W\sqrt{Z}v_{\mathbf{k}}\right\rangle_0. \tag{79}$$

The matrix m describes the effective energy needed to create a bond fermion of specific type and spin: A bond fermion blocks other hopping processes and affects the renormalization constant $\sqrt{Z}$, so in the effective Hamiltonian creation processes are punished. Λ_0 holds the Lagrange multipliers $\Lambda_{\sigma\sigma'}^0$.

To investigate antiferromagnetic, ferromagnetic, and incommensurate order, we numerically minimize the variational energy for fixed external parameters t', J, and n_c. The minimization is implemented through three nested loops, listed from outermost to innermost:

(1) Optimization of the variational energy as a function of the triplet background. We call this energy $E_{\text{var}}(|\mathbf{t}|, \mathbf{Q})$, as all other properties of the wave function can be calculated from these two input values (along with the external parameters). This is a low-dimensional nonlinear optimization problem, which we solve using an algorithm from the free software suite NLOPT.

(2) Calculation of $E_{\text{var}}(|\mathbf{t}|, \mathbf{Q})$ for given input values. This can be done in multiple ways, but our calculation follows Yao [50]. We guess (mostly arbitrary) starting values for $\sqrt{Z}$ and m, find the ground state of the resulting effective Hamiltonian (76), and then calculate new values of $\sqrt{Z}$ and m through (69) and (79). We iterate this procedure a few times to find an approximate solution, which we use as a starting value for the MINPACK nonlinear equation solver. $E_{\text{var}}(|\mathbf{t}|, \mathbf{Q})$ is then calculated through (71).

(3) For fixed $\sqrt{Z}$ and m, the effective Hamiltonian (76) still depends on the Lagrange multiplier matrix Λ. Its elements have to be solved for to enforce (54), which we again do using MINPACK.

As there are multiple competing phases in the model, we performed local optimizations with different starting values for $|\mathbf{t}|$ and $\mathbf{Q}$. For example, one set of starting parameters corresponds to the "small Fermi surface" antiferromagnetic phase (which has a larger $|\mathbf{t}|$), while a different one corresponds to the "large Fermi surface" antiferromagnetic phase (which has a smaller $|\mathbf{t}|$). Momentum integrals are taken as sums over an equally spaced grid, with a fictional effective temperature $T = 0.001t$. Changing the grid size or decreasing the temperature had no significant effect on our results.

IV. ANTIFERROMAGNETIC PHASE DIAGRAM

We first focus on the case of pure antiferromagnetic ordering with only nearest neighbor hopping, which corresponds to fixing $\mathbf{Q} = (\pi, \pi)$ and $t' = 0$. This is the most symmetric and most well-studied setting. While our method also allows us to perform calculations in the more general case, it is reassuring to first show that we can reproduce the main features of the model that have been established in previous investigations, with quantitative improvements over the previous bond fermion theory [42]. Incommensurate and ferromagnetic ordering will be discussed in a later section.

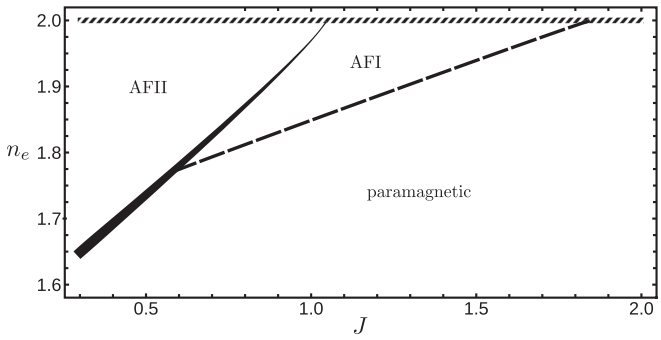

FIG. 1. The phase diagram when taking into account only antiferromagnetic and paramagnetic phases. The dashed line indicates the (second-order) transition to the magnetic AFI phase, the full line the (first-order) transition to the AFII phase. The thickness of the full line schematically follows the size of the jump in the magnetic parameter $|\mathbf{t}|$. At half-filling $n_e = 2$ (striped line), the transition becomes continuous. Furthermore, the system is gapped for all J at half-filling.

When varying J and n_c, three different phases emerge (Fig. 1). At large J, formation of magnetic moments is suppressed by the interaction which favors singlets ($\mathbf{t} = 0$). Two antiferromagnetic phases (we will refer to them as AFI and AFII) are found for moderate J: The symmetry of the magnetic ordering is the same in both cases, but away from half-filling ($n_c \neq 1$) there is a discontinuous drop in $|\mathbf{t}|$ across the transition from AFII to AFI (Fig. 2). The difference between the phases lies in their band structures (Fig. 3), which as usual we approximate through the eigenvalues of the effective Hamiltonian [50]. The Fermi surfaces are shown in Fig. 4. Note that the only $\mathbf{k}$ dependence in the effective Hamiltonian is through $\epsilon_{\mathbf{k}\pm\frac{\mathbf{Q}}{2}}$ in (28), which for $t' = 0$ satisfies $\epsilon_{\mathbf{k}+\frac{\mathbf{Q}}{2}} = -\epsilon_{\mathbf{k}-\frac{\mathbf{Q}}{2}}$, so there is only a single free parameter. The Fermi surfaces must thus be lines of constant $\epsilon_{\mathbf{k}}$. As the Fermi surfaces of a trivially solvable free-electron ($J = 0$) system follow these same lines (with $\epsilon_{\mathbf{k}} = E_{\text{Fermi}}$, the Fermi energy), the sheets of the interacting Fermi surface can be identified with those of a free-electron system. However, this associated

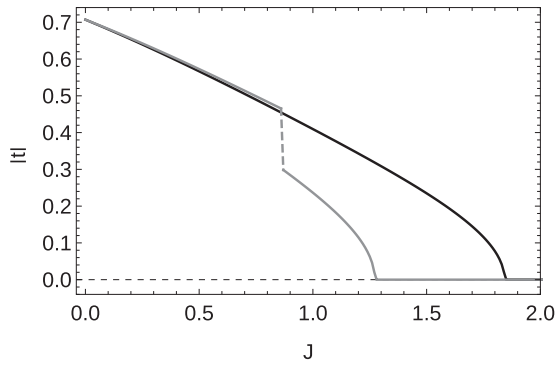

FIG. 2. The magnetic order parameter $|\mathbf{t}|$ at $n_c = 1$ (black) and $n_c = 0.9$ (gray). The transition to the paramagnetic phase with $|\mathbf{t}| = 0$ shows a square-root behavior. At half-filling, $|\mathbf{t}|$ is continuous (the critical point $J_{c,2} = 1.04t$ for the AFI-AFII transition is not distinct), while away from half-filling there is a jump in $|\mathbf{t}|$ (dashed gray line).

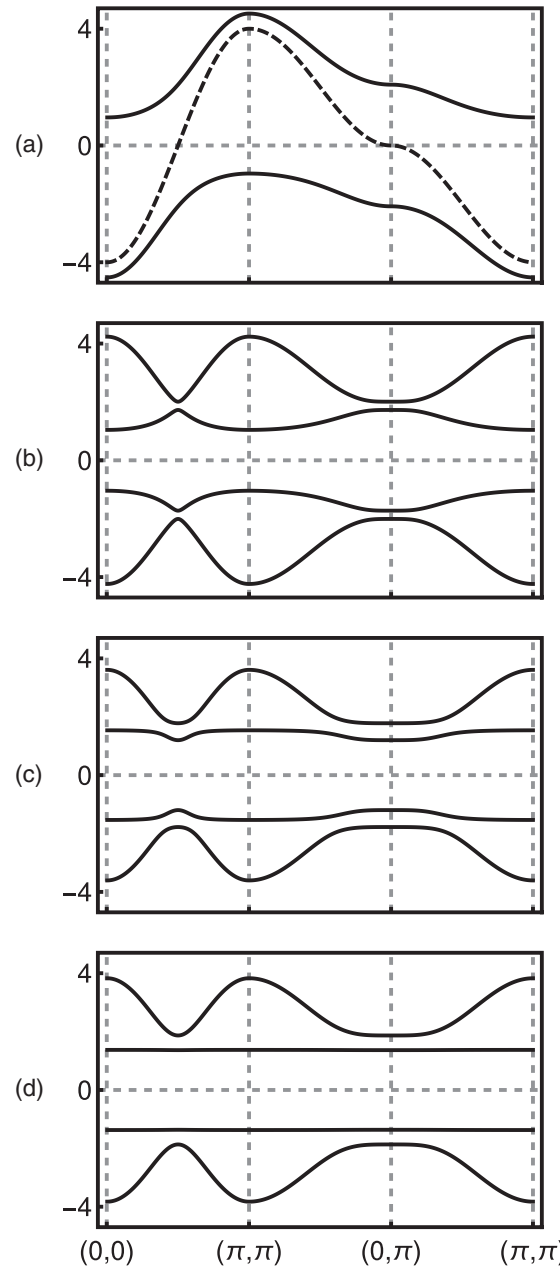

FIG. 3. The excitation band structure at half-filling for different values of J. (a) Paramagnetic phase (black, $J = 2t$), with the free band structure for comparison (dashed). (b) AFI phase $J = 1.6t$. (c) AFII phase $J = 0.7t$. (d) Near the critical point $J = 1.04t$.

noninteracting system does not necessarily need to have the same electron density as the original Kondo lattice model.

The paramagnetic and AFI phases have heavy hole pockets around (π, π) [and for AFI at the magnetically backfolded (0,0)]. This is usually dubbed the "large" Fermi surface phase, as the Fermi surface is that of a noninteracting tight-binding system filled with $n_e = n_c + 1$ itinerant electrons: The usual interpretation is that the f electrons (despite being localized) still contribute to the Fermi surface volume. Meanwhile, the AFII ("small" Fermi surface) has the same Fermi surface as a noninteracting system filled with n_c itinerant electrons (the f electrons "drop out"), albeit with somewhat heavier bands and

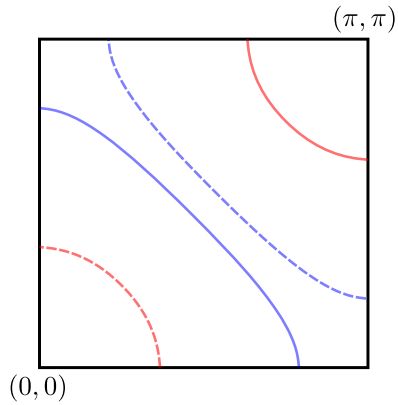

FIG. 4. The possible Fermi surfaces at $n_c = 0.8$. The full red line is the noninteracting system's Fermi surface if it was filled with $n_c = 1.8$ electrons. It is also the Fermi surface of the large-J paramagnetic phase, so the localized electrons can be interpreted as contributing 1 electron. The AFI phase's Fermi surface is identical to the paramagnetic one, except for the antiferromagnetic folding (red dashed). The full blue line corresponds to the noninteracting system with $n_c = 0.8$ electrons. This (together with the blue dashed line) is also the Fermi surface for the AFII phase, showing that only the actual conduction electrons contribute to the Fermi surface. An explanation as to why the interacting Fermi surfaces coincide with those of a noninteracting (free-electron) system can be found in the main text.

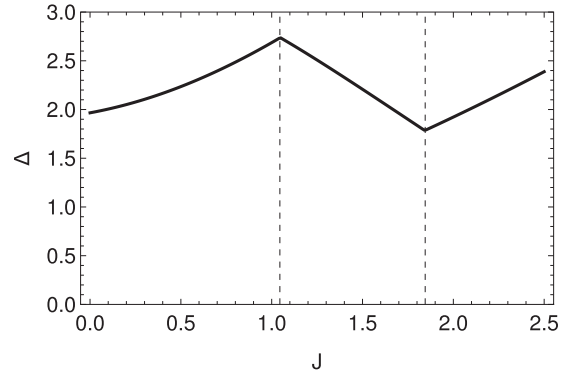

FIG. 5. The size of the gap Δ (defined as the minimum distance between the two bands surrounding the gap) at half-filling. The gap does not close in the noninteracting ($J = 0$) limit as excitations still block each other. For $J \gg 1$ (not shown), we get $\Delta \to \frac{3}{2}J$, the energy needed to destroy two singlets. The kinks in Δ coincide respectively with the AFII-AFI and AFI-paramagnetic phase transitions (dashed lines).

antiferromagnetically folded. This behavior of the bands is qualitatively very similar to the results of DCA and QMC [30]. While real-space DMFT predicts non-Néel ordered states, there is a very similar transition in Fermi surface topology there as well [33].

Approaching half-filling, all three phases develop band gaps (Fig. 5). For large J, this gap is simply the energy required to break up two singlets and create two bond fermion excitations, while at small J this corresponds to a magnetic gap (with no clear transition between the two limits). A limitation of our method (and the related one of Jurecka and Brenig [40]) is that the $J \to 0$ limit is not the expected free-electron system (with the localized spins completely decoupled from the conduction band). From the start we have excluded three of the four single-occupation states from our variational ansatz, which is not a reasonable assumption for $J = 0$. From this, we must expect a gap of order t even at $J = 0$, as a quasiparticle excitation blocks a site from participating in electron transport, and the kinetic energy per site is of order t. Speaking more quantitatively, the exact ground-state energy of the $J = 0$ system is $E_{\text{exact}} = -16/\pi^2 t = -1.62t$. Our result compares poorly with the variational energy $E_{\text{var}} = -1.08t$. With such a sizable discrepancy, we cannot expect to make even qualitative predictions for small J.

Luckily, the region of antiferromagnetic phase transitions is found at moderate J, where our approximations are easier to justify. At half-filling, the critical value for the transition to magnetic order is $J_c = 1.85t$, which is a lot closer to the QMC value of $J_c = 1.45t$ than the original bond fermion result of $J_c = 2.3t$ [42]. To compare, the VMC of Watanabe and Ogata gives a value of $J_c = 1.7t$ [27]. In our view, this represents something of a "gold standard" for calculations that do not explicitly include long-range fluctuations (the wave function of Watanabe and Ogata consists of an uncorrelated state multiplied by a purely local projection operator). From this standpoint, the accuracy of the bond fermion prediction for J_c appears adequate. We also note that DMFT gives $J_c = 2.2t$ [33], and DCA $J_c = 2.1t$ [31], while series expansion in t/J results in $J_c = 1.48t$ [25,26].

A mean-field description gives the critical value as $J_c = 0.4W = 3.2t$ ($W = 8t$ is the free bandwidth) [17]. The mean-field ground-state energy will be close to the true value for $J \ll t$, but for $J \gg t$ the energy per site is only $-\frac{3}{8}J$ instead of $-\frac{3}{4}J$ (the Kondo singlet is a correlated state), which matches that J_c comes out larger by a factor of roughly two compared to other calculations. Mean-field theory is thus accurate in the opposite limit as bond fermion theory, with a crossover in the ground-state energy somewhere in between. Zhang and Yu performed a similar calculation for a generalized anisotropic version of the Kondo lattice [11]: When specialized to the isotropic case, they give a value $J_c = 1.16t$, but calculated under the assumption of a flat density of states.

The bond fermion theory of Jurecka and Brenig [40] deserves special consideration; we elaborate on their results in Appendix B.

An interesting property of the phase diagram is that the AFI-AFII-transition in a sense exists even at half-filling. There are no Fermi surfaces due to the gap, but the change in the band structure can still be detected. A "peak" in the valence band at the $\epsilon_{\mathbf{k}} = 0$ line [which contains $(\pi/2, \pi/2)$ for example] flips and turns into a "trough." Away from half-filling, this is accompanied by the aforementioned discontinuous change in Fermi surface (Lifshitz transition). While there is no Lifshitz transition at half-filling, the change in band structure still occurs. In this sense, half-filling is "smoothly connected" to the doped case, as on each side of the AFI-AFII-transition the chemical potential simply wanders into the gap when approaching half-filling.

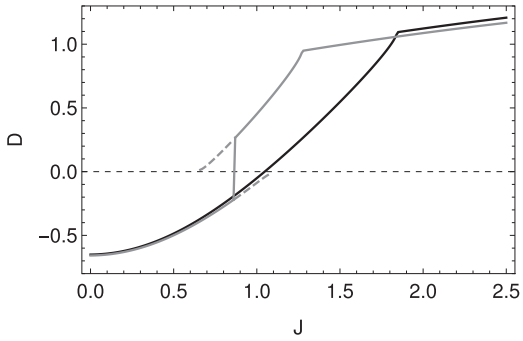

FIG. 6. $D = E_v(0,0) - E_v(\pi/2, \pi/2)$ for $n_c = 1$ (black) and $n_c = 0.9$ (gray). Here, $E_v(\mathbf{k})$ is the quasiparticle energy in the second lowest (valence) band, so that $|D|$ is the width of the valence band. Compare Figs. 3(b)–3(d): D changes sign at the transition between AFI and AFII. The density of states ν (and the effective mass) behave as $\nu \propto 1/|D|$. This means that there is a divergence in the half-filled case, while in a doped system there is a jump. The kink near $J = 1.9t$ ($J = 1.3t$) corresponds to the transition to the paramagnetic phase.

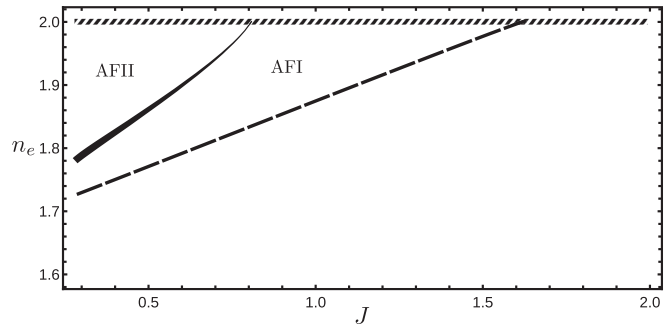

FIG. 7. Same as Fig. 1, but for $t' = 0.4t$.

A further consequence of the gap is that the AFI-AFII transition itself is also smooth at half-filling: In the doped regime, there is a jump in $|\mathbf{t}|$ because of the Lifshitz transition. With a gap, the flipping of the band structure can happen continuously, without a jump in $|\mathbf{t}|$. Even more dramatically, at the critical point $J_{c,2} = 1.04t$ (when the maximum turns into a minimum), the whole band is perfectly flat [Fig. 3(d)]. Intuitively, we can imagine moving an infinitesimal distance away from half-filling. On either side of the transition the Fermi surface is locked to either the red or the blue lines in Fig. 4, so for a continuous phase transition the surface must be ill defined at $J_{c,2}$. Exactly this happens at the flat band. A rigorous mathematical treatment is found in Appendix C.

This should not be confused with a decoupling of the c and f electrons (as appears, for example, in Hartree-Fock calculations at small J [17]). In our ansatz, localized and delocalized electrons are coupled no matter the phase. Rather, the flat band arises at the critical point between two phases, one of which is dominated by c electrons (AFII) and the other by f electrons (AFI).

It is to be emphasized that this leads to a divergent density of states and band mass at the transition point. While the square lattice is pathological in the sense that even in the free system the DOS diverges at zero energy, this is "only" logarithmic [a consequence of the saddle point of $\epsilon_{\mathbf{k}}$ for $k = (0, \pi)$ and similar points], while in our case the two bands around the gap are each compressed into zero-width slivers. In fact, the symmetries that lead to the flat band (most significantly that $\epsilon_{\mathbf{k}+\frac{\mathbf{Q}}{2}} = -\epsilon_{\mathbf{k}-\frac{\mathbf{Q}}{2}}$; see Appendix C) are also present in the nonpathological three-dimensional cubic lattice, so we expect a similar situation to occur there also.

At finite doping, the band becomes narrower close to the transition, but a perfectly flat band is not realized. Instead, the DOS increases when approaching the transition from either side, but does not diverge (Fig. 6). Around the critical point there is a coexistence region with two separate local minima in the energy, corresponding to each of the antiferromagnetic phases. One of these minima is only metastable, and the transition is the point where their energies cross. As shown in the figure, the valence band becomes very narrow for both phases in their respective metastable regions, but the transition occurs before a flat band is realized. We speculate that even at finite doping, inclusion of long-range fluctuations may move the phase transition closer toward these regions, as a large DOS would enhance them. As discussed in Sec. VI, some heavy fermion magnetic transitions show a significant (likely divergent) mass enhancement near the phase transition.

We will now also briefly discuss the $t' \neq 0$ case. The phase diagram is qualitatively similar, although the antiferromagnetic regions become smaller (Fig. 7). In particular, the size of the AFII phase is reduced, which can be interpreted as a consequence of the decreased nesting in the free band structure. The two magnetic phases can again be recognized by their qualitatively differing Fermi surfaces (Figs. 8 and 9). However, since the lattice is no longer bipartite and particle-hole symmetry is broken, one can no longer directly identify the Fermi surfaces with those of a free system. $\epsilon_{\mathbf{k}\pm\frac{\mathbf{Q}}{2}}$ are essentially independent quantities and act as two different $\mathbf{k}$-dependent parameters in the effective Hamiltonian, so the hole pockets do not have to follow lines of constant $\epsilon_{\mathbf{k}}$. The AFII Fermi is no longer ring-like, surrounding the center of the Brillouin zone, but instead consists of disconnected hole pockets at $(\pi/2, \pi/2)$ and symmetrically equivalent positions. Still, the AFI-AFII transition is similar to before, as the maximum near $(\pi/2, \pi/2)$ flips around at the transition. One must note that due to the reduced symmetry, the conduction band no longer becomes globally flat at the critical point, but there remains a line of almost dispersionless excitations along the diagonal of the Brillouin zone [Fig. 8(d)]. The density of states will thus still drastically increase near the transition point.

V. FERROMAGNETIC AND INCOMMENSURATE PHASES

We now turn our attention to the more general case of arbitrary $\mathbf{Q}$. This includes the already discussed antiferromagnetic phases, but also ferromagnetism [$\mathbf{Q} = (0, 0)$] and more general spiral order. It turns out that all phases except AFI are unstable against such non-Néel ordering. The resulting phase diagram is pictured in Fig. 10. Notably, the paramagnetic phase is replaced by ferromagnetism (FM). The other major change is in the area previously occupied by the small Fermi surface AFII phase, which is replaced by a sequence of phases with nontrivial $\mathbf{Q}$:

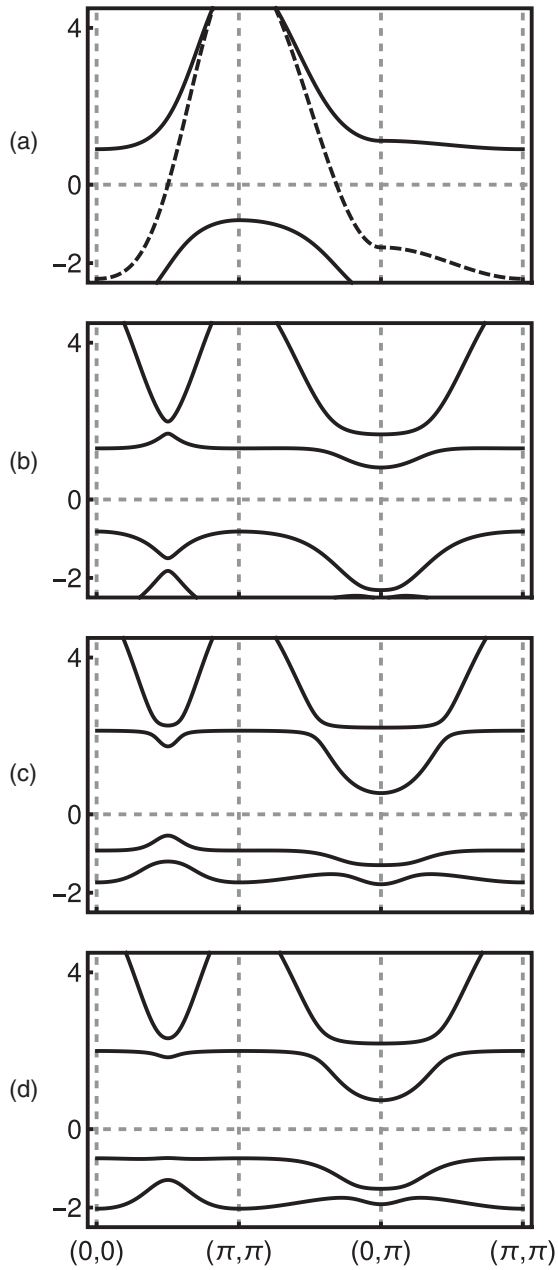

FIG. 8. Analogous to Fig. 3, but for $t' = 0.4t$. (a) Paramagnetic phase (black, $J = 1.62t$), with the free band structure for comparison (dashed). (b) AFI phase $J = 1.3t$. (c) AFII phase $J = 0.5t$. (d) Close to the critical point $J = 0.82t$.

(1) ID: incommensurate phase with a wave vector lying along a *diagonal* of the Brillouin zone, $\mathbf{Q} = (q, q)$.

(2) IE: incommensurate phase with a wave vector lying along an *edge* of the Brillouin zone, $\mathbf{Q} = (q, \pi)$.

(3) S: commensurate phase with *stripe* magnetic order along a coordinate axis, $\mathbf{Q} = (0, \pi)$.

Pure antiferromagnetism remains only at half-filling, and in the AFI phase. More generally, the situation at half-filling is completely unchanged, and the two critical interaction values have the same values as before.

We will now discuss possible explanations for the appearance of each of these phases, beginning with the FM phase.

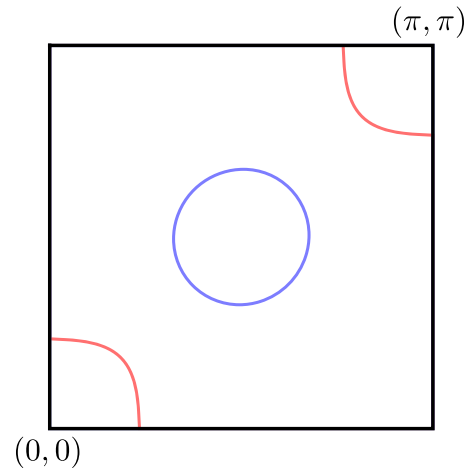

FIG. 9. The Fermi surfaces for $t' = 0.4t$ and $n_c = 0.9$ Unlike the $t' = 0$ case (Fig. 4), the lines do not follow any equipotential lines, so they cannot be directly matched to free band structures. Pictured are AFI in red ($J = 0.5t$) and the AFII in blue ($J = 0.62t$).

Close to half-filling, the band structure is qualitatively identical to the paramagnetic phase, except for a splitting of the bands (Fig. 11). In fact, the splitting is always strong enough to completely polarize the Fermi surface, resulting in one conducting and one insulating band. This type of "spin-selective" Kondo insulator has previously been proposed by Peters *et al.* in both infinite dimensions [35] and in one dimension [36] (in the latter case, perturbatory expansion in t/J leads to a rigorous proof of ferromagnetism in the $J \to \infty$ limit [51]). The tell-tale sign of this phase is the identity (if we assume $\downarrow$ to be the minority carrier) $n^c_\downarrow = n^f_\uparrow$. Intuitively, each minority c electron is bound to an f electron of opposite spin. This condition is fulfilled here as well. The same phase was also found in two dimensions [17,34].

The results of these studies differ from ours in that ferromagnetism is only present at low conduction electron concentration $n_c \lesssim 0.5$, whereas in our calculation polarization is present at arbitrarily small doping. From a purely mathematical standpoint, it seems that the FM phase is caused by a Stoner-like mechanism aided by the large density of

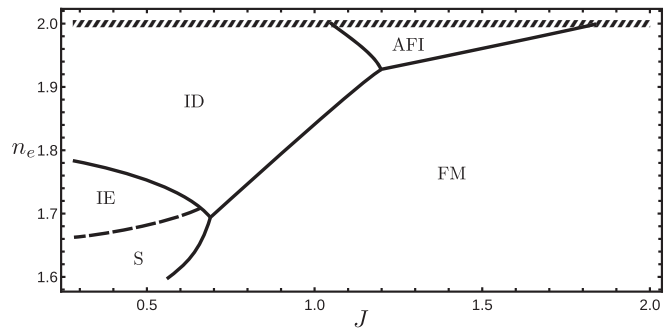

FIG. 10. Phase diagram with incommensurate and ferromagnetic phases. The dashed line indicates a second-order transition; all other transitions are discontinuous. Explanations of each phase can be found in the main text.

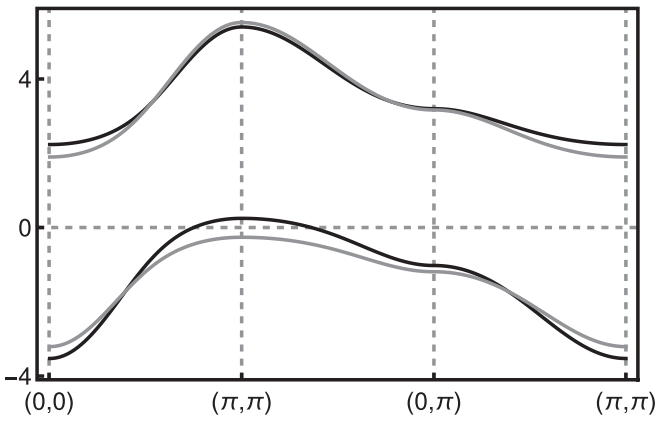

FIG. 11. The band structure in the ferromagnetic (FM) phase with $n_c = 0.9$ and $J = 2.02t$. The majority (minority) spins are in black (gray).

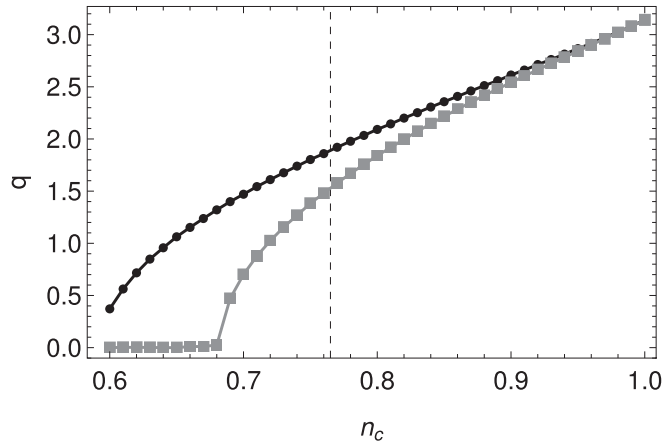

FIG. 12. The evolution of $\mathbf{Q}$ for fixed $J = 0.5t$ at varying doping. The black (gray) shows the optimal q when $\mathbf{Q}$ is restricted to the diagonal (edge) of the Brillouin zone, where q is respectively defined through $\mathbf{Q} = (q, q)$ and $\mathbf{Q} = (q, \pi)$. The vertical line signifies the phase transition: to the right, the diagonal (ID) phase has lower energy; to the left, the edge (IE) phase. For $q = 0$ or $q = \pi$, we have commensurate magnetic order.

states of the very heavy conduction band. A small ferromagnetic admixture to the triplet background is only weakly punished by the Heisenberg interaction, but increases hopping processes for the polarized bond fermions. Furthermore, the number of hard-core collisions is reduced by a polarization of the conduction bands. Only at quite large $J \sim 8t$ does the Heisenberg interaction win out and the system becomes paramagnetic. This seems to be a consistent feature of the bond fermion theory as similar behavior was found for the triangular lattice [43].

While this ferromagnetic phase at small doping seems unphysical to us, we can very roughly judge how "far off" we are from the more likely paramagnetic solution. For this, we turn to previous DCA [32] and Gutzwiller approximation [38] studies, where the model was investigated with an applied magnetic field. In both cases, the magnetization profile was qualitatively similar: With increasing B field the magnetization quickly saturated, with a *metamagnetic* transition at larger field strength. The fully polarized ferromagnetic phase we have found corresponds to the saturated region. While quantitative comparisons are difficult, the figures in the references indicate that the magnetic field needed for saturation is quite small: In the DCA calculation at $n_c = 0.9$, $J = 1.3t$, and a ratio of Landé factors $g_f/g_c = 4$, the magnetization saturates at $B \approx 0.002t$. In the Gutzwiller calculation at $n_c = 0.88$, $J = 0.45D$ (where D is the half-bandwidth, in our case $4t$), and Landé factors $g_f = g_c$, $B = 0.01D$ is already in the saturated region. We take these small values of the magnetic field needed for full polarization as a sign that even at low doping the Kondo lattice is energetically quite close to the fully polarized ferromagnetic state. The likely reason for the appearance of ferromagnetism in bond fermion theory is that our calculation does not take triplet fluctuations into account.

We now turn to the incommensurate phases. Doping away from half-filling with $J < J_{c,2}$, $\mathbf{Q}$ smoothly moves away from the Néel vector (π, π), toward the origin along the diagonal of the Brillouin zone (Fig. 12). This forms the ID phase. For $J \gtrsim 0.6t$, further doping leads directly to a phase transition to FM. In the case of small J, one instead first finds another incommensurate phase of different symmetry, where $\mathbf{Q}$ jumps toward the edge of the Brillouin zone (IE). From there, the system transitions smoothly to a commensurate phase of the form $\mathbf{Q} = (0, \pi)$: The magnetic moments are laid out in alternating stripes with inequivalent x and y axes (S).

We can compare these results to the mean-field calculations of Costa *et al.* [17] and Pankratova *et al.* [18], which should be reasonably accurate for small J. While Costa *et al.* allow for c-f hybridization, this is only relevant in phases featuring Kondo screening. In our region of interest, their calculation is equivalent to that of Pankratova *et al.*, except that the latter allow for phase separation. As we have not investigated phase separation ourselves, we will focus on the results of Costa *et al.*

The bond fermion and mean-field phase diagrams are similar to a point, as the mean-field theory also predicts two different kinds of antiferromagnetism and stripe magnetism. However, there are significant quantitative differences. For example, as Fig. 12 shows, when fixing $J = 0.5t$ the crossover between the ID and IE phases occurs near $n_c = 0.76$ in our calculation. For Costa *et al.*, the transition always occurs for $n_c > 0.9$ even at larger $J = 0.3W = 2.4t$.

Effectively, the bond fermion method heavily amplifies the effect of the local moments for smaller J. Similar to how the system is still gapped for $n_c = 1$ and $J = 0$, the choice of $\mathbf{Q}$ still influences the strength of the hopping even for a small or vanishing J. From this standpoint, it may actually be a positive surprise that, even in the region where the bond fermion wave function is not an appropriate ansatz, our phase diagram is still comparable to the mean-field result. However, we must assume that the ID phase is in truth confined to a much smaller region that in our phase diagram, the IE phase growing larger in turn. For another opinion, one can consult the DMFT results of Peters and Kawakami [34]. While they did not investigate incommensurate order, they also support the existence of a striped magnetic phase near $n_c = 0.5$.

VI. DISCUSSION AND SUMMARY

The bond fermion method is a strong-coupling approximation; i.e., it is initially justified in the limit of infinite interaction. Instead of focusing on c and f electrons, we try and guess at the significant excitation modes (the bond fermions) to then extend the calculation to finite interaction. In this way, we see it as an ansatz complementary to mean-field theory, which is more natural at small interaction. The draw of the bond fermions is that it allows us to work solely with *physical* states, meaning that the condition of single occupancy on the f electrons is fulfilled simply by the nature of the ansatz. We believe this to be significant because this condition is "dense," as for a generic wave function of c and f electrons around half of all lattice sites will not actually fulfill it. One will need to introduce a different (necessarily approximate) method to alleviate this problem.

Of course, this has to be evaluated relative to the simplifications we in turn had to impose in order to solve the system. For one, we still had to use a Gutzwiller approximation of our own to implement the hard-core interaction of the bond fermions. However, we think this aspect is not as significant a drawback as it may seem at first glance. The condition is "dilute," in the sense that (unless far from half-filling) the bond fermion concentration ρ_{BF} is typically around 0.1 to 0.2 per site in our calculation, and the probability of a double occupancy scales with ρ_{BF}^2. A more pressing issue is disregarding triplet (bosonic) fluctuations. Some attempts to accommodate them have been made in the paramagnetic phase [41], but it is so far unclear to us how to include them in our variational framework. For small J (where our method is currently inapplicable), introducing bond operators for triplets would lead to a very strongly correlated, computationally intractable system. However, we guess that deficiencies at moderate to large J, like the ferromagnetic phase close to half-filling, may be cured with the right approach.

While the Kondo lattice is generally seen as providing a good description of basic heavy-fermion physics, it is clear that such simple model cannot adequately describe phase transitions in real materials. Rather, the model appears to have a variety of phases which differ only very little in their energy, so that small additional terms will determine which phase is realized. In the following, we thus want to give a few examples where actual heavy fermion compounds show a behavior which is reminiscent of results obtained above. One example is $CeRh_{1-x}Co_xIn_5$, which has the quasilayered $HoCoGa_5$ structure [52] and thus may approximately be described by the two-dimensional Kondo lattice model. In fact, this material shows similarities to the phase diagram obtained above [53]. Ignoring its superconducting phase, the compound shows commensurate Néel order within the a-b planes, but incommensurate order along the c axis at $x = 0$. Doping first leads to a transition to another antiferromagnetic phase with three-dimensional Néel order and a reconstructed Fermi surface, and then to a paramagnetic phase. Fermi surface imaging suggests that the f electrons are localized in the incommensurate phase, while after the reconstruction they should be included in the Fermi surface volume. Superficially, this mirrors some aspects of our phase diagram, as we can find analogues of these phases in our calculations. The incommensurate phase would correspond to either IE or ID (which both have a small Fermi surface) and the commensurate one to the AFI phase (large Fermi surface). If we start out in IE/ID and assume codoping to be equivalent to increasing J/t, we have a similar sequence of phase transitions to the experiment. At the first transition, the Fermi surface is reconstructed to include the f electrons, and the ordering vector becomes commensurate. Magnetic order as a whole vanishes later, at a second transition.

However, the analogy is imperfect. Instead of in-plane spiral order as in our two-dimensional description, the incommensurability is in the out-of-plane direction with a wave vector $\mathbf{Q} = (\pi/a, \pi/a, q/c)$. Further, unlike our calculation, no sign of a significant narrowing of the bands was found near the transition.

If one instead takes pure $CeRhIn_5$ and applies pressure, one gets a direct transition from incommensurate antiferromagnetism to paramagnetism [54], with no intermediate commensurate state. According to our calculation, this is also possible in the Kondo lattice, albeit only at lower electron densities. What is particularly interesting here is that while the De Haas–Van Alphen frequencies of each band seem to be almost constant on each side of the transition (indicating that the Fermi surface does not change much), some of the effective masses seem to diverge. This is unlike the doping-induced transition, and fits with our observation that the Fermi surface reconstruction is associated with a significant flattening of the valence band near the transition. A similar pressure-induced transition was observed in $CeRh_2Si_2$ as well [55], also featuring the mass enhancement.

A different, much-studied example for incommensurate magnetic order is given by the system $CeCu_2(Si_{1-x}Ge_x)_2$ [56–59]. This compound has the layered $ThCr_2Si_2$ structure and the Fermi surface takes the form of warped cylinders [56] so that a description by a planar model may be reasonable. This system shows incommensurate magnetic order with an ordering vector close to $\mathbf{Q} = (\pi/2a, \pi/2a, \pi/c)$, whereby the ordered moment forms a spiral in the plane perpendicular to $\mathbf{Q}$ [57]. It has to be noted, however, that in $CeCu_2Si_2$ the ordering vector has been shown [56] to correspond to a nesting vector of the heavy quasiparticle Fermi surface obtained for the paramagnetic phase by the renormalized band structure method. In this picture, the antiferromagnetic phase would correspond to a spin-density-like instability of the "large" Fermi surface, that is the AFI phase in the present theory. This interpretation would therefore not be consistent with the present theory, where the incommensurate phase replaces the AFII phase.

In summary, we have improved the bond fermion method for the Kondo lattice by combining it with a Gutzwiller approximation step. When restricted to Néel ordering, this qualitatively reproduces previous phase diagrams, featuring two antiferromagnetic phases distinguished through a reconstruction of the Fermi surface. The critical value for the onset of magnetic order at half-filling was calculated to be $J_c = 1.85t$, a significant improvement over the previous method. When allowing for more general planar ordering, one of the antiferromagnetic phases is replaced by a series of states with incommensurate ordering vectors, similar to mean-field results [17].

ACKNOWLEDGMENT

The authors acknowledge support by the state of Baden-Württemberg through bwHPC.

APPENDIX A: SUM RULES AND PHYSICALITY OF EXPECTATION VALUES

As in other interaction systems, sum rules for electron expectation values are a useful tool to evaluate the validity of approximations. Clearly, we should try to preserve these rules as much as possible, as violations would point to inconsistencies in approximations. More specifically, previous presentations of bond fermion methods used some *ad hoc* measures to ensure the equality between local electron density and **k**-integrated electron number [39,42]. We will here explain how these details are handled in the present paper.

For simplicity, it is enough to consider the paramagnetic case (i.e., $s = 1$, $\mathbf{t} = 0$). Let us try to evaluate how electrons are distributed over **k**-modes. For this, we introduce the Green's function

$$G_{\sigma\sigma'}(\mathbf{R},\mathbf{R}') = \langle c^\dagger_{\mathbf{R}\sigma} c_{\mathbf{R}'\sigma'}\rangle \tag{A1}$$

$$= G(\mathbf{R}-\mathbf{R}')\delta_{\sigma\sigma'}, \tag{A2}$$

$$G(\mathbf{R}-\mathbf{R}') = \langle c^\dagger_{\mathbf{R}\uparrow} c_{\mathbf{R}'\uparrow}\rangle. \tag{A3}$$

This gives the local electron density for $\mathbf{R} = \mathbf{R}'$. From Sec. II, we find that G is given through two different expressions depending on $\mathbf{R}$ and $\mathbf{R}'$. For $\mathbf{R} \neq \mathbf{R}'$, (46) should be used. The result is

$$G(\mathbf{R}-\mathbf{R}') = \tfrac{1}{2}\langle b^\dagger_{\mathbf{R}\uparrow} b_{\mathbf{R}'\uparrow}\rangle + \tfrac{1}{2}\langle a_{\mathbf{R}\downarrow} a^\dagger_{\mathbf{R}'\downarrow}\rangle - \tfrac{1}{2}\langle b^\dagger_{\mathbf{R}\uparrow} a^\dagger_{\mathbf{R}'\downarrow}\rangle - \tfrac{1}{2}\langle a_{\mathbf{R}\downarrow} b_{\mathbf{R}'\uparrow}\rangle \tag{A4}$$

$$= G'(\mathbf{R}-\mathbf{R}'). \tag{A5}$$

We introduced the "nonlocal" Green's function G' in the final line, which we understand to be defined through the same expression even for $\mathbf{R} = \mathbf{R}'$. It will give the **k** dependence of the electron occupation numbers. Meanwhile, for the "true" Green's function we have [using (42)]

$$G(\mathbf{R}-\mathbf{R}') = \begin{cases} G'(\mathbf{R}-\mathbf{R}') & \mathbf{R} \neq \mathbf{R}' \\ \frac{1}{2} - \langle a^\dagger_{\mathbf{R}\uparrow} a_{\mathbf{R}\uparrow}\rangle + \langle b^\dagger_{\mathbf{R}\uparrow} b_{\mathbf{R}\uparrow}\rangle & \mathbf{R} = \mathbf{R}' \end{cases}. \tag{A6}$$

One can see that in general, $G \neq G'$ for $\mathbf{R} = \mathbf{R}'$. As explained in the main text, expectation values of pairing terms like $\langle b^\dagger_{\mathbf{R}\uparrow} a^\dagger_{\mathbf{R}'\downarrow}\rangle$ must vanish due to the hard-core constraint, with which (A4) gives

$$G(\mathbf{0}) = G'(\mathbf{0}) - \tfrac{1}{2}\langle a^\dagger_{\mathbf{R}\uparrow} a_{\mathbf{R}\uparrow}\rangle + \tfrac{1}{2}\langle b^\dagger_{\mathbf{R}\uparrow} b_{\mathbf{R}\uparrow}\rangle. \tag{A7}$$

We get the **k**-space occupation numbers by Fourier transforming G:

$$\langle c^\dagger_{\mathbf{k}\uparrow} c_{\mathbf{k}\uparrow}\rangle = G(\mathbf{k}) \tag{A8}$$

$$= \sum_{\mathbf{R}} e^{i\mathbf{k}\mathbf{R}} G(\mathbf{R}). \tag{A9}$$

We can split this sum into a local and a nonlocal part, resulting in

$$G(\mathbf{k}) = \sum_{\mathbf{R}\neq\mathbf{0}} e^{i\mathbf{k}\mathbf{R}} G'(\mathbf{R}) + G(\mathbf{R}=\mathbf{0}) \tag{A10}$$

$$= G'(\mathbf{k}) - G'(\mathbf{R}=\mathbf{0}) + G(\mathbf{R}=\mathbf{0}). \tag{A11}$$

The number of electrons in the **k** mode is thus given by $G'(\mathbf{k})$, with the second and third term giving a constant offset.

Upon averaging (A11) over **k**, the first two terms cancel and the third remains unchanged. Thus, the **k** sum rule for the total electron density is fulfilled.

A subtle point about (A11) is that we need to be careful about how to enforce the hard-core condition on the bond fermions. $G(\mathbf{k})$ gives the number of electrons in a momentum state **k**, so clearly

$$0 \leqslant G(\mathbf{k}) \leqslant 1. \tag{A12}$$

This *physicality rule* is automatically enforced as long as all bond fermion expectation values are evaluated on an *admissible* state, i.e., one that obeys the hard-core constraint. For a generic state, however, (A11) can lead to violations of (A12) and result in negative or too-large occupation numbers, which is clearly undesirable. This should be kept in mind when solving the system approximately.

We have checked for a variety of parameters whether the Gutzwiller approximation of the main text fulfills the physicality rule, and we have found no violations. While we have been unable to prove this in general, from the limit of infinite dimensions we consider this to be sensible. Since the Gutzwiller approximation is exact in infinite dimensions, it is sure to produce a state fulfilling (A12). As the dimensionality enters the approximation only indirectly through the density of states, we expect the physicality rule to hold also in finite dimensions.

While the hard-core condition was disregarded in some previous works [39,42,43], the physicality rule was in fact obeyed. One can check from (A5) that the rule holds for G' by itself even on inadmissible states, i.e., $0 \leqslant G'(\mathbf{k}) \leqslant 1$ no matter whether the hard-core condition is enforced. One way to enforce physicality is thus to require

$$G(\mathbf{R}=\mathbf{0}) = G'(\mathbf{R}=\mathbf{0}) \Rightarrow G(\mathbf{k}) = G'(\mathbf{k}), \tag{A13}$$

for which a Lagrange multiplier λ was introduced [39].

APPENDIX B: THE TECHNIQUE OF JURECKA AND BRENIG

A different bond fermion method was introduced by Jurecka and Brenig [40,41]. Here, the translation between electrons and bond particles happens entirely on the operator level. Instead of choosing a particular "ground state" Ω, the bond particle operators act on a vacuum state that does not correspond to any state in the original Hilbert space. All local states of the Kondo lattice are treated on a similar footing by introducing bond bosons $s^\dagger_{\mathbf{R}}$ and $\mathbf{t}^\dagger_{\mathbf{R}}$ to generate the singlet S and the triplet $\mathbf{T}$ (bosonic commutation rules are natural as these are states with an even number of electrons). The result is an exact (but interacting) mapping of the Kondo lattice model, provided the physicality condition

$$1 = a^\dagger_{\mathbf{R}} a_{\mathbf{R}} + b^\dagger_{\mathbf{R}} b_{\mathbf{R}} + s^\dagger_{\mathbf{R}} s_{\mathbf{R}} + \mathbf{t}^\dagger_{\mathbf{R}} \mathbf{t}_{\mathbf{R}} \tag{B1}$$

is enforced (each site must be in exactly one physical state).

For actual calculations, the bosons were considered to be condensed, with (B1) fulfilled on average. The condensation amplitudes $\langle s_{\mathbf{R}}\rangle$ and $\langle \mathbf{t}_{\mathbf{R}}\rangle$ correspond to our parameters $s_{\mathbf{R}}$ and $t_{\mathbf{R}}$ from Sec. II. However, unlike our description, these

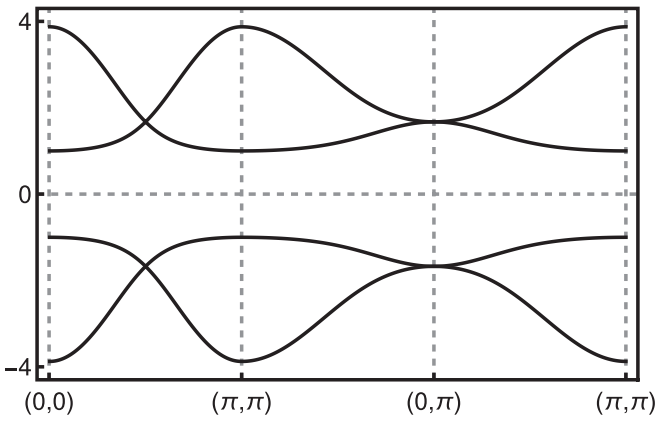

FIG. 13. The band structure at half-filling and $J = 1.1t$ (the antiferromagnetic phase), calculated using the method of Jurecka and Brenig. Note the band crossing at $(\pi/2, \pi/2)$.

amplitudes are not normalized to unity. Instead of (15), the condition (B1) results in

$$|\langle s_{\mathbf{R}}\rangle|^2 + |\langle \mathbf{t}_{\mathbf{R}}\rangle|^2 = 1 - \langle a^\dagger_{\mathbf{R}} a_{\mathbf{R}}\rangle + \langle b^\dagger_{\mathbf{R}} b_{\mathbf{R}}\rangle. \tag{B2}$$

The kinetic energy contribution is quadratic in $\langle s_{\mathbf{R}}\rangle$ and $\langle \mathbf{t}_{\mathbf{R}}\rangle$; see (48). The smaller values of these amplitudes thus result in an automatic renormalization of the band structure. For an equivalent calculation in the language of the present paper, we normalize the parameters to unity as in the main text, but define

$$\sqrt{Z} = \sqrt{1 - \langle a^\dagger a\rangle + \langle b^\dagger b\rangle}, \tag{B3}$$

with no matrix structure in spin or bond fermion space. This result can alternatively be derived from our own formulation by treating the hard-core constraint using Barnes' original slave boson mean field theory [60] instead of the Gutzwiller approximation.

While the result for the critical interaction strength is impressive ($J_c = 1.5t$ at $n_c = 1$ close to the QMC result of $1.45t$), there are issues. It is not clear what is to be done about expectation values of the pair creation terms $\langle a^\dagger_{\mathbf{R}\sigma} b^\dagger_{\mathbf{R}\sigma'}\rangle$. Nonzero expectation values were implicitly accepted in the Jurecka-Brenig calculation; as an alternative, one can use a Lagrange multiplier matrix Λ (as in the main text) to set them to zero.

We have performed some calculations using the Jurecka-Brenig theory using both of these options. In either case, the only antiferromagnetic phase we could find was the large Fermi surface state (AFI), both at half-filling and for the doped system. Let us first discuss the calculation without Λ (or equivalently, fixing $\Lambda = 0$).

In fact, the underlying reason for the lack of a phase transition was already mentioned by Jurecka and Brenig [40]. Looking at the band structure in the antiferromagnetic phase (Fig. 13), one notices that the lower (upper) bands touch each other at $(\pi/2, \pi/2)$. This should be compared with Fig. 3(b) in the main text, where a gap between the bands is visible. The discrepancy exists because in the Jurecka-Brenig method the antiferromagnetic scattering in the effective Hamiltonian is also proportional to $\epsilon_{\mathbf{k}}$. For $(\pi/2, \pi/2)$, we have $\epsilon_{\mathbf{k}} = 0$, so the bands do not repel. Accordingly, the mechanism of the band minimum at $(\pi/2, \pi/2)$ turning into a maximum is also impossible, and the AFII phase cannot be obtained.

In the language of the present paper (where the magnetic vector points in the x direction), these scattering terms are precisely the spin-flip terms in the effective Hamiltonian. In (76), such terms appear as the off-diagonal terms of m and in Λ, which result in a band coupling (and thus repulsion) independent of $\mathbf{k}$. Of these, m is numerically much more important, as it corresponds to scattering between touching bands, while Λ scatters between bands separated by the energy gap. The Jurecka-Brenig theory in contrast has a diagonal m, owing to the complete symmetry of (B1).

Choosing the second option (meaning, adding Λ) results only in a very small correction to the band structure. This is too little to induce the Lifshitz transition. It also changes the position of the critical point to $J_c = 1.3t$, less accurate the previous result.

APPENDIX C: MATHEMATICAL DETAILS CONCERNING THE FLAT BAND

At half-filling and $t' = 0$, one can exploit a variety of symmetries. For example, we have $\mathbf{Q} = (\pi, \pi)$ and thus $\epsilon_{k+\frac{\mathbf{Q}}{2}} = -\epsilon_{k-\frac{\mathbf{Q}}{2}}$ in (28). From (76), one gets the 4×4 band structure Hamiltonian

$$H_{\mathbf{k}} = h + \epsilon_{k+\frac{\mathbf{Q}}{2}} K, \tag{C1}$$

$$K = -\sqrt{Z} W^\intercal \begin{pmatrix} 1 & 0 \\ 0 & -1 \end{pmatrix} W \sqrt{Z}. \tag{C2}$$

The matrices h and K are functions of the Gutzwiller parameters $\sqrt{Z}$ and m obtained from solving the self-consistency equation, and the value of $|\mathbf{t}|$ from the minimization. As such, they are implicitly functions of J. Note that they do not depend on $\mathbf{k}$, and the only momentum dependence is in $\epsilon_{k+\frac{\mathbf{Q}}{2}}$.

The band energies are the eigenvalues of $H_{\mathbf{k}}$. At $J_{c,2} = 1.04t$, one finds that one pair of eigenvalues is constant, meaning independent of $\epsilon_{k+\frac{\mathbf{Q}}{2}}$. However, an explicit numerical calculation shows that h and K neither commute nor anticommute (in fact, $hK \pm Kh$ both have full rank). From this, one can infer that there is no $\mathbf{k}$-independent transformation to (block-)diagonalize $H_{\mathbf{k}}$. This illustrates why the flat band does not correspond to a physical symmetry: The symmetry operation involves both a translation in $\mathbf{k}$ space as well as a rotation in the abstract bond fermion space.

To give some mathematical insight into the circumstances required for the flat band, we calculate the eigenvalues E^* as the roots of the characteristic polynomial $p(E)$. We can infer the form (abbreviating $\epsilon_{k+\frac{\mathbf{Q}}{2}}$ as ϵ)

$$p(E) = \det(E - H_{\mathbf{k}}) \tag{C3}$$

$$= \det(E - h - \epsilon K) \tag{C4}$$

$$= \sum_{0 \leqslant i+j \leqslant 4} c_{ij}(h, K) E^i \epsilon^j. \tag{C5}$$

Since the characteristic polynomial of a $N \times N$ matrix is a polynomial in its entries (of total degree N), we can write $p(E)$ as a degree four polynomial in E and ϵ. It is clear that for a generic polynomial, the roots of $p(E)$ (as a function of

E) will surely depend on ϵ, and there will be no flat bands. The question is now how many degrees of freedom actually remain in the coefficients c_{ij}. As we only have J left as an external parameter, we will need to show that the existence of the flat band is equivalent to tuning J to the root of a single (complicated) function $f(J)$.

The particle-hole symmetry implies that the roots E^* of $p(E)$ are symmetric about zero, which implies that only terms even in E appear. Further, from the derivation in Sec. II, one can see that flipping the sign of ϵ (or rather exchanging $k + \frac{\mathbf{Q}}{2} \leftrightarrow k - \frac{\mathbf{Q}}{2}$) is the same as flipping spin up and spin down, which should not have any effect as the magnetic moments are located in the x-y plane. As a result, $p(E)$ must also be even in ϵ. Thus $c_{ij} \neq 0$ only if i and j are both even.

To proceed further, we consider the limits $\epsilon = 0$ and $\epsilon \to \infty$. They respectively yield

$$\sum_{0 \leqslant i \leqslant 4} c_{i0}(h, K)E^i = \det(E - h), \tag{C6}$$

$$c_{04}(h, K) = \det(K) = 0. \tag{C7}$$

The second equality in (C7) follows from (C2): K is a 4×4 matrix, but its definition also includes the 2×4 matrix W. If we take a (four-dimensional) vector v so that $\sqrt{Z}v$ is orthogonal to both vectors corresponding to the two rows of W, we have $Kv = 0$. Thus, K must be singular.

Putting these things together, we get

$$p(E) = \det(E - h) + c_{02}\epsilon^2 + c_{22}E^2\epsilon^2. \tag{C8}$$

We now set E to one of the eigenvalues of h, $E^*(h)$. This results in

$$p(E^*(h)) = \epsilon^2\left(c_{02} + c_{22}E^*(h)^2\right) \tag{C9}$$

$$= \epsilon^2 f(J). \tag{C10}$$

If we can tune J so that $f(J)$ vanishes, the right side will be identically zero. Thus, $E^*(h)$ is a root of the characteristic polynomial independent of ϵ and forms a flat band.

Of course, if and where such roots occur depends on c_{02} and c_{22}, which are complicated functions of J. In our calculation, we have one root at $J = 1.04t$, the transition point from AFII to AFI.

In summary, the following conditions facilitate the existence of the flat band:

(1) The effective Hamiltonian is only four-dimensional.

(2) Particle-hole symmetry reduces the number of independent eigenvalues.

(3) The kinetic energy matrix K has a zero mode.

[1] Q. Si and F. Steglich, Science **329**, 1161 (2010).
[2] S. Doniach, Phys. B: Condens. Matter **91**, 231 (1977).
[3] J. Kondo, Prog. Theor. Phys. **32**, 37 (1964); K. G. Wilson, Rev. Mod. Phys. **47**, 773 (1975).
[4] M. A. Ruderman and C. Kittel, Phys. Rev. **96**, 99 (1954); T. Kasuya, Prog. Theor. Phys. **16**, 45 (1956); K. Yosida, Phys. Rev. **106**, 893 (1957).
[5] J. R. Schrieffer and P. A. Wolff, Phys. Rev. **149**, 491 (1966).
[6] A. Yoshimori and A. Sakurai, Prog. Theor. Phys. Suppl. **46**, 162 (1970).
[7] C. Lacroix and M. Cyrot, Phys. Rev. B **20**, 1969 (1979).
[8] C. Lacroix, J. Magn. Magn. Mater. **100**, 90 (1991).
[9] A. Auerbach and K. Levin, Phys. Rev. Lett. **57**, 877 (1986).
[10] S. Burdin, A. Georges, and D. R. Grempel, Phys. Rev. Lett. **85**, 1048 (2000).
[11] G.-M. Zhang and L. Yu, Phys. Rev. B **62**, 76 (2000).
[12] M. Lavagna and C. Pepin, Phys. Rev. B **62**, 6450 (2000).
[13] T. Senthil, M. Vojta, and S. Sachdev, Phys. Rev. B **69**, 035111 (2004).
[14] M. Vojta, Phys. Rev. B **78**, 125109 (2008).
[15] G.-M. Zhang, Y.-H. Su, and L. Yu, Phys. Rev. B **83**, 033102 (2011).
[16] J. Nilsson, Phys. Rev. B **83**, 235103 (2011).
[17] N. C. Costa, J. P. Lima, and R. R. dos Santos, J. Magn. Magn. Mater. **423**, 74 (2017).
[18] A. K. Pankratova, P. A. Igoshev, and V. Y. Irkhin, J. Phys. Soc. Jpn. **33**, 375802 (2021).
[19] C. C. Yu and S. R. White, Phys. Rev. Lett. **71**, 3866 (1993).
[20] S. Moukouri and L. G. Caron, Phys. Rev. B **52**, 15723(R) (1995).
[21] S. Moukouri and L. G. Caron, Phys. Rev. B **54**, 12212 (1996).
[22] T. Mutou, N. Shibata, and K. Ueda, Phys. Rev. Lett. **81**, 4939 (1998).
[23] S. Smerat, U. Schollwock, and I. P. McCulloch, and H. Schoeller, Phys. Rev. B **79**, 235107 (2009).
[24] F. F. Assaad, Phys. Rev. Lett. **83**, 796 (1999).
[25] Z.-P. Shi, R. R. P. Singh, M. P. Gelfand, and Z. Wang, Phys. Rev. B **51**, 15630(R) (1995).
[26] W. Zheng and J. Oitmaa, Phys. Rev. B **67**, 214406 (2003).
[27] H. Watanabe and M. Ogata, Phys. Rev. Lett. **99**, 136401 (2007).
[28] M. Z. Asadzadeh, F. Becca, and M. Fabrizio, Phys. Rev. B **87**, 205144 (2013).
[29] K. Kubo, J. Phys. Soc. Jpn. **84**, 094702 (2015).
[30] L. C. Martin and F. F. Assaad, Phys. Rev. Lett. **101**, 066404 (2008).
[31] L. C. Martin, M. Bercx, and F. F. Assaad, Phys. Rev. B **82**, 245105 (2010).
[32] M. Bercx and F. F. Assaad, Phys. Rev. B **86**, 075108 (2012).
[33] R. Peters and N. Kawakami, Phys. Rev. B **92**, 075103 (2015).
[34] R. Peters and N. Kawakami, Phys. Rev. B **96**, 115158 (2017).
[35] R. Peters, N. Kawakami, and T. Pruschke, Phys. Rev. Lett. **108**, 086402 (2012).
[36] R. Peters and N. Kawakami, Phys. Rev. B **86**, 165107 (2012).
[37] T. Sato, F. F. Assaad, and T. Grover, Phys. Rev. Lett. **120**, 107201 (2018).
[38] N. Lanatà, P. Barone, and M. Fabrizio, Phys. Rev. B **78**, 155127 (2008).
[39] R. Eder, O. Stoica, and G. A. Sawatzky, Phys. Rev. B **55**, R6109 (1997).
[40] C. Jurecka and W. Brenig, Phys. Rev. B **64**, 092406 (2001).
[41] R. Eder, Phys. Rev. B **99**, 085134 (2019).
[42] R. Eder, K. Grube, and P. Wróbel, Phys. Rev. B **93**, 165111 (2016).
[43] M. Keßler and R. Eder, Phys. Rev. B **102**, 235125 (2020).
[44] J. Hubbard, Proc. R. Soc. London, Ser. A **276**, 238 (1963).

[45] V. N. Kotov, O. Sushkov, W. Zheng, and J. Oitmaa, Phys. Rev. Lett. **80**, 5790 (1998).
[46] M. C. Gutzwiller, Phys. Rev. Lett. **10**, 159 (1963).
[47] W. Metzner and D. Vollhardt, Phys. Rev. B **37**, 7382 (1988).
[48] G. Kotliar and A. E. Ruckenstein, Phys. Rev. Lett. **57**, 1362 (1986).
[49] M. Fabrizio, Phys. Rev. B **76**, 165110 (2007).
[50] Y. X. Yao, J. Schmalian, C. Z. Wang, K. M. Ho, and G. Kotliar, Phys. Rev. B **84**, 245112 (2011).
[51] M. Sigrist, H. Tsunetsugu, K. Ueda, and T. M. Rice, Phys. Rev. B **46**, 13838 (1992).
[52] H. Hegger, C. Petrovic, E. G. Moshopoulou, M. F. Hundley, J. L. Sarrao, Z. Fisk, and J. D. Thompson, Phys. Rev. Lett. **84**, 4986 (2000).
[53] S. K. Goh, J. Paglione, M. Sutherland, E. C. T. O'Farrell, C. Bergemann, T. A. Sayles, and M. B. Maple, Phys. Rev. Lett. **101**, 056402 (2008).
[54] H. Shishido, R. Settai, H. Harima, and Y. Ōnuki, J. Phys. Soc. Jpn. **74**, 1103 (2005).
[55] S. Araki, R. Settai, T. C. Kobayashi, H. Harima, and Y. Ōnuki, Phys. Rev. B **64**, 224417 (2001).
[56] O. Stockert, E. Faulhaber, G. Zwicknagl, N. Stüsser, H. S. Jeevan, M. Deppe, R. Borth, R. Küchler, M. Loewenhaupt, C. Geibel, and F. Steglich, Phys. Rev. Lett. **92**, 136401 (2004).
[57] G. Knopp, A. Loidl, K. Knorr, L. Pawlak, M. Duczmal, R. Caspary, U. Gottwick, H. Spille, F. Steglich, and A. P. Murani, Z. Phys. B **77**, 95 (1989).
[58] G. Knebel, C. Eggert, D. Engelmann, R. Viana, A. Krimmel, M. Dressel, and A. Loidl, Phys. Rev. B **53**, 11586 (1996).
[59] N. Oeschler, M. Deppe, E. Lengyel, R. Borth, P. Gegenwart, G. Sparn, C. Geibel, and F. Steglich, Phys. Rev. B **71**, 094409 (2005)
[60] S. E. Barnes, J. Phys. F **6**, 1375 (1976); **7**, 2637 (1977).